

**Supplement to The 1-way on-line coupled model system
MECO(n) – Part 4: Chemical evaluation (based on MESSy
v2.52)**

Mariano Mertens
Institut für Physik der Atmosphäre
DLR-Oberpfaffenhofen

`mariano.mertens@dlr.de`

August 2016

Contents

S1 Supplementary figures	3
S1.1 Dry deposition rates	3
S1.2 On-line calculated emissions of soil-NO _x and isoprene	5
S1.3 Annual cycle of ozone at different stations	6
S1.4 Taylor diagrams with non 'height corrected' results	8
S1.5 Nitrogen dioxide concentrations for June 2008	9
S1.6 Nitric acid concentrations	10
S1.7 Isoprene mixing ratios	12
S1.8 Vertical ozone profiles	14
S2 Comparison with ERA-Interim	19
S2.1 CM50	19
S2.2 CM12	27
S3 Comparison with temperature profiles from ozone sondes	30
S3.1 CM50	30
S4 COSMO-Namelist	33
S4.1 'lmgrid'-namelist	33
S4.2 'runctl'-namelist	34
S4.3 'tuning'-namelist	36
S4.4 'dyncontrol'-namelist	37
S4.5 'phycontrol'-namelist	39
S5 List of used stations	41
S6 Detailed list of used submodels	44
S7 References	46

S1 Supplementary figures

S1.1 Dry deposition rates

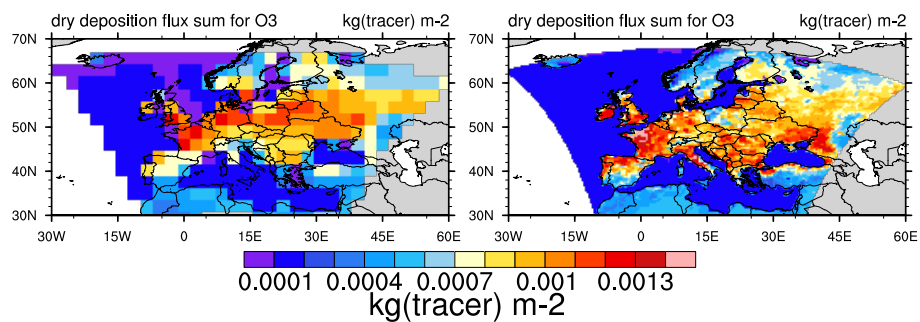


Figure S1: Dry deposition sum for June 2008 of ozone (in kg m^{-2}) from EMAC (left) and COSMO (right). Over Poland less ozone is deposited in COSMO compared to EMAC. This is due to different soil types in both models.

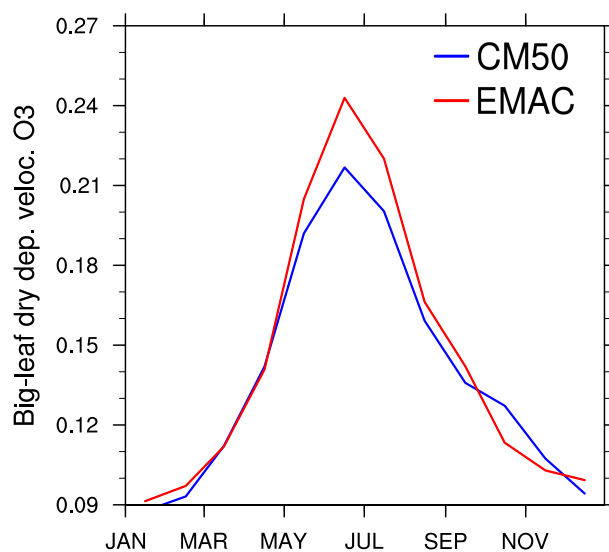


Figure S2: Monthly area weighted average dry deposition flux velocity (in cm s^{-1}) for EMAC and COSMO.

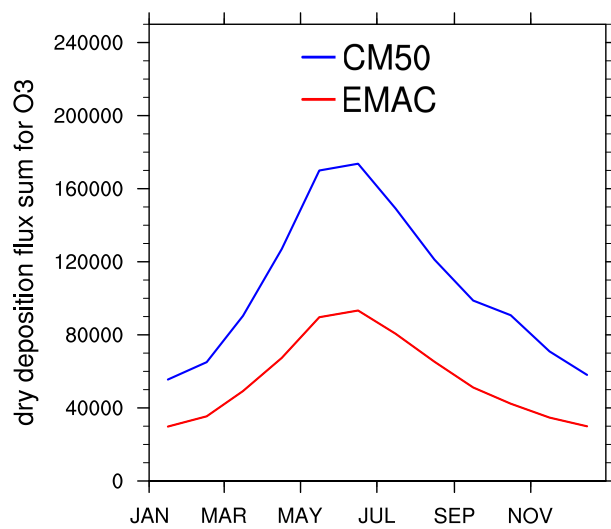


Figure S3: Monthly averaged dry deposition flux (in kg O₃) from EMAC and COSMO.

S1.2 On-line calculated emissions of soil-NO_x and isoprene

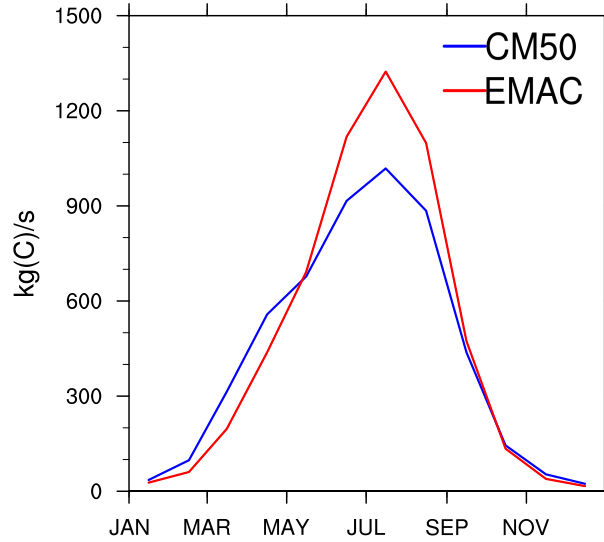


Figure S4: Monthly averaged on-line emissions of isoprene (in kg(C) s⁻¹). The emissions are summed over all gridboxes within the domain of the CM50 instance (neglecting the relaxation area). Please note, that the unscaled emissions are plotted.

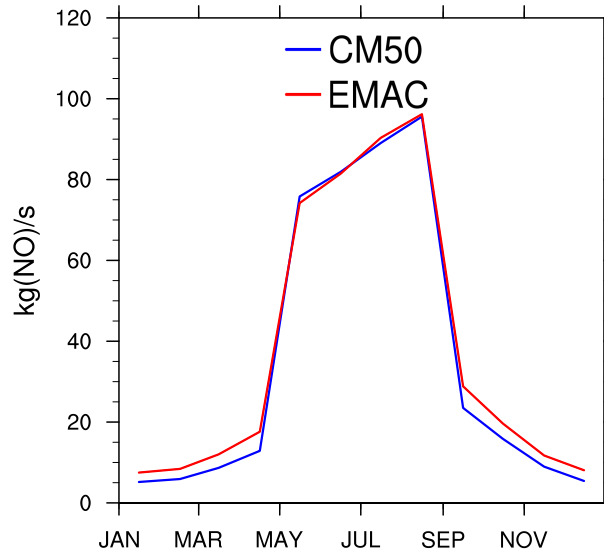


Figure S5: Monthly averaged on-line emissions of soil-NO_x (in kg(NO) s⁻¹). The emissions are summed over all gridboxes within the domain of the CM50 instance (neglecting the relaxation area). The increase of the emissions in the period from May - August are mainly due to the fact, that the algorithm assumes increased fertilization of agricultural areas in this period.

S1.3 Annual cycle of ozone at different stations

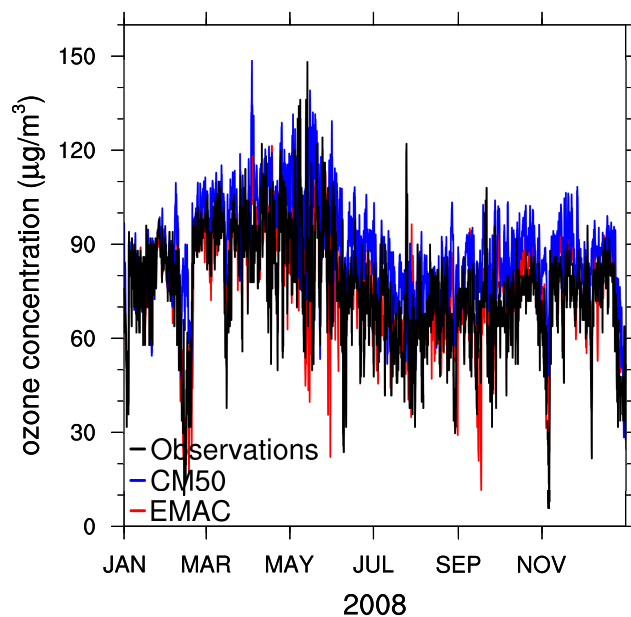


Figure S6: Box-smoothed (7 days) average of ozone concentration (observed and simulated) at the Mace Head station in Ireland.

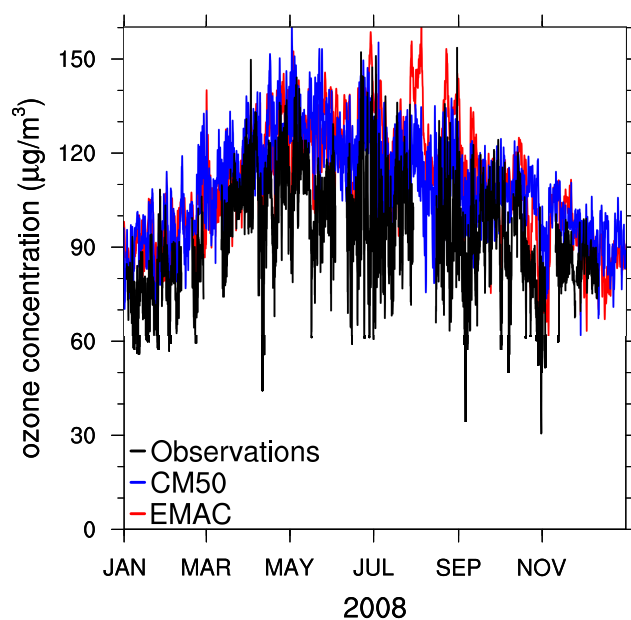


Figure S7: As Fig. S6 but for Giordan Lighthouse, Malta.

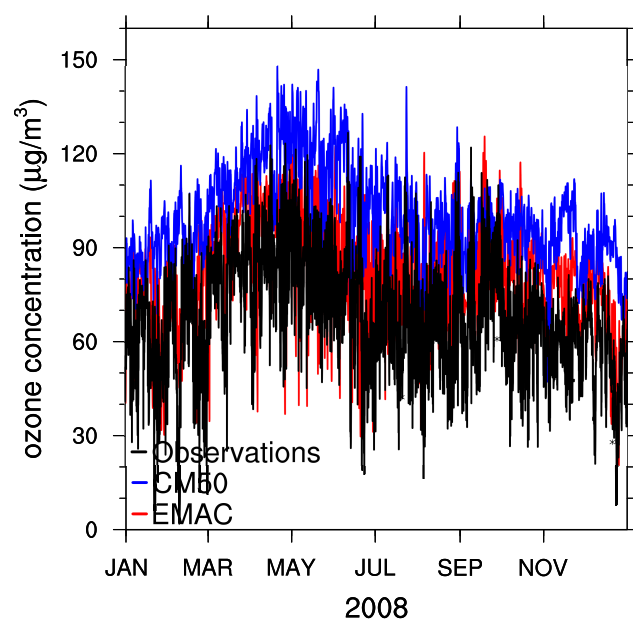


Figure S8: As Fig. S6 but for Niembro, Spain.

S1.4 Taylor diagrams with non 'height corrected' results

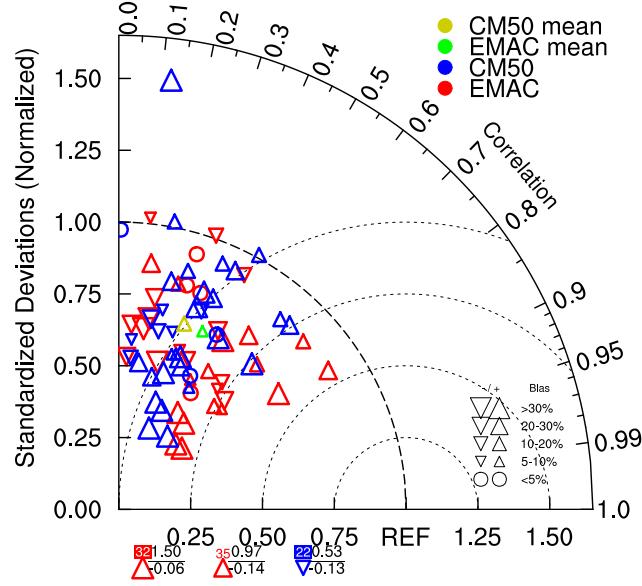


Figure S9: Taylor diagram for ground level ozone concentrations in June 2008. The results for EMAC are indicated in red, for COSMO/MESSy in blue. The mean over all stations is coloured in green for EMAC and in golden colour for COSMO/MESSy. The size of the symbols indicate the bias in percent; upward symbols show a positive bias, downward symbols a negative bias. In difference to the Taylor diagram in the main manuscript the non height corrected values are used here.

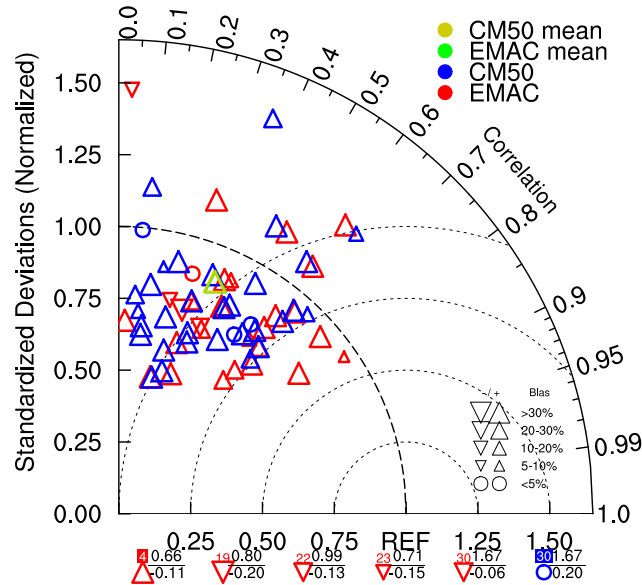


Figure S10: As Fig. S9 but for December 2008.

S1.5 Nitrogen dioxide concentrations for June 2008

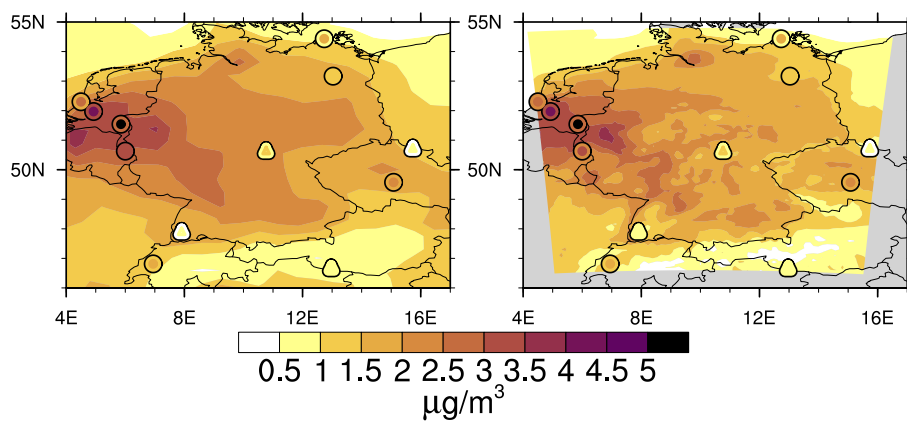


Figure S11: Monthly averaged nitrogen dioxide concentrations in $\mu\text{g (N) m}^{-3}$ from CM50 (left) and CM12 (right) at the lowest model layer for June 2008. The inner part of the coloured dots depicts the monthly mean values measured at the corresponding stations, while the outer part shows the simulated value corrected for the station height.

S1.6 Nitric acid concentrations

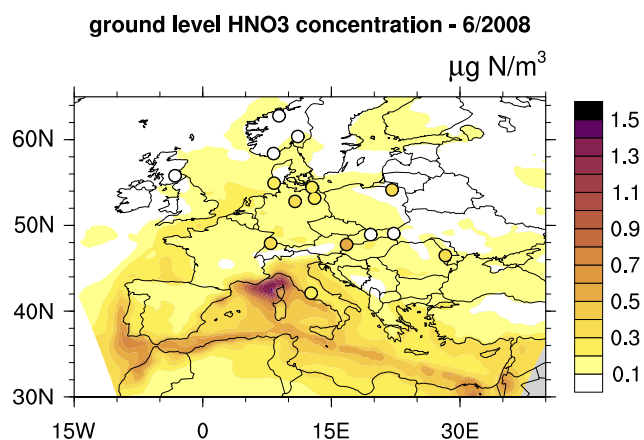


Figure S12: Monthly averaged nitric acid concentrations in $\mu\text{g (N) m}^{-3}$ from CM50 at the lowest model layer for June 2008. The coloured dots depicts the monthly mean values measured at the corresponding stations.

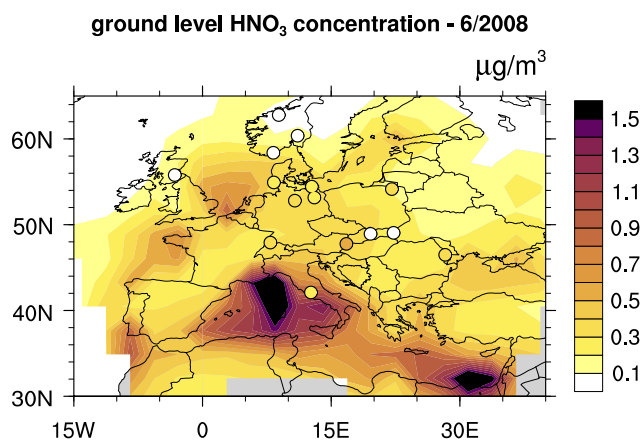


Figure S13: As figure S12 but for EMAC.

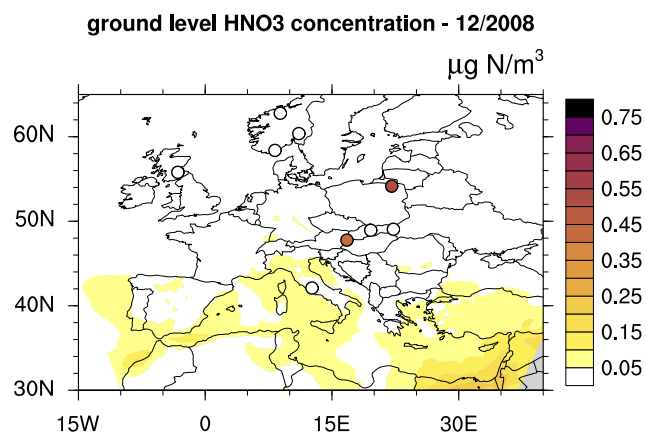


Figure S14: Monthly averaged nitric acid concentrations in $\mu\text{g (N) m}^{-3}$ from CM50 at the lowest model layer for December 2008. The coloured dots show the monthly mean values measured at the corresponding stations.

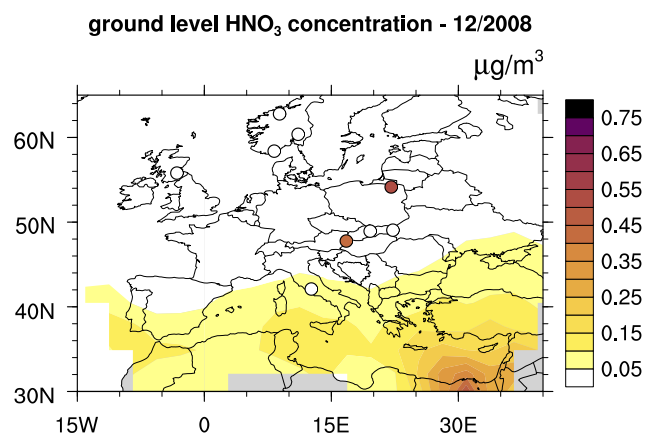


Figure S15: As Fig. S14 but for EMAC.

S1.7 Isoprene mixing ratios

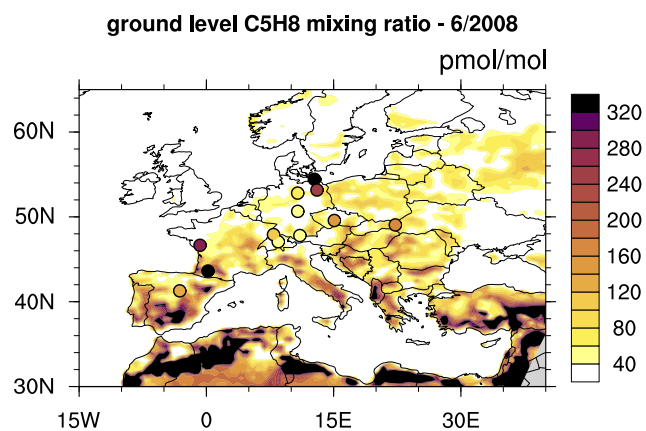


Figure S16: Monthly averaged isoprene mixing ratios in pmol mol^{-1} from CM50 at the lowest model layer for June 2008. The coloured dots show the monthly mean values measured at the corresponding stations.

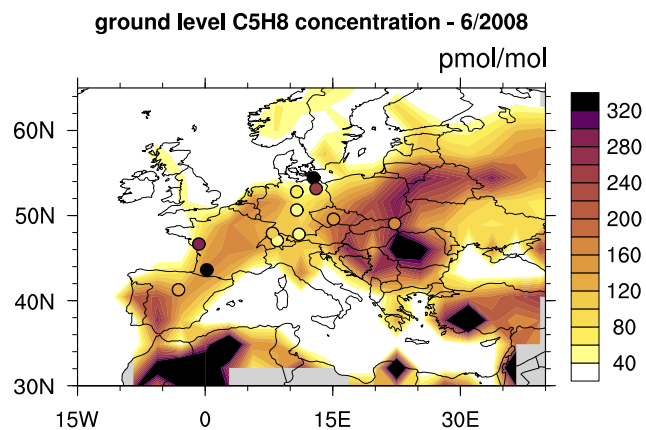


Figure S17: As Fig. S16 but for EMAC.

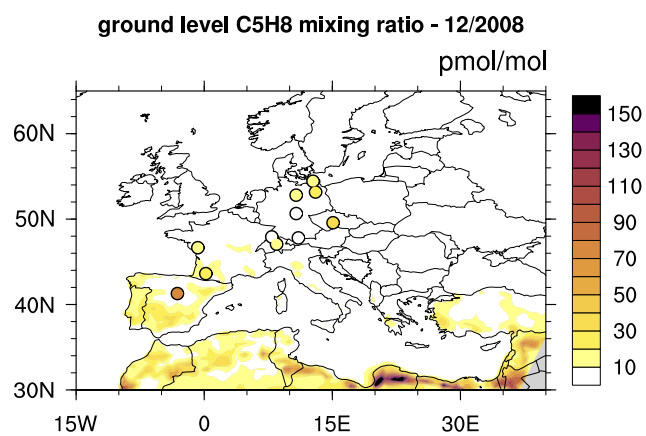


Figure S18: Monthly averaged isoprene mixing ratios in pmol mol^{-1} from CM50 at the lowest model layer for June 2008. The coloured dots show the monthly mean values measured at the corresponding stations.

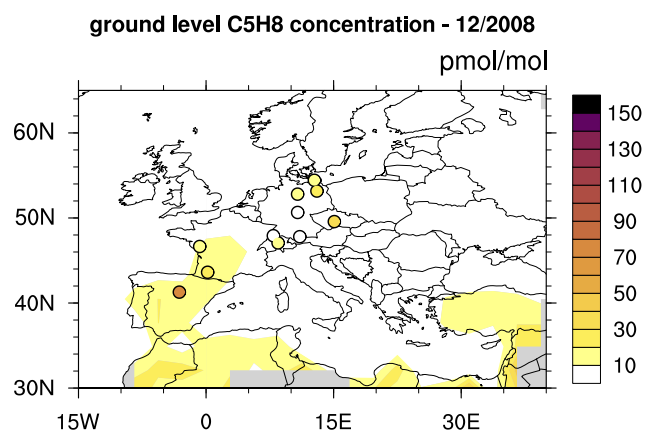


Figure S19: As Fig. S18 but from EMAC.

S1.8 Vertical ozone profiles

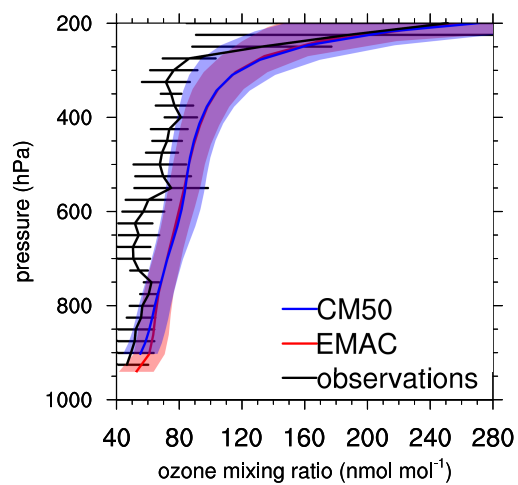


Figure S20: Vertical ozone profile at Madrid for June 2008. The standard deviation of the temporal mean is indicated by the error bars for the observations and by the shaded area for the model data.

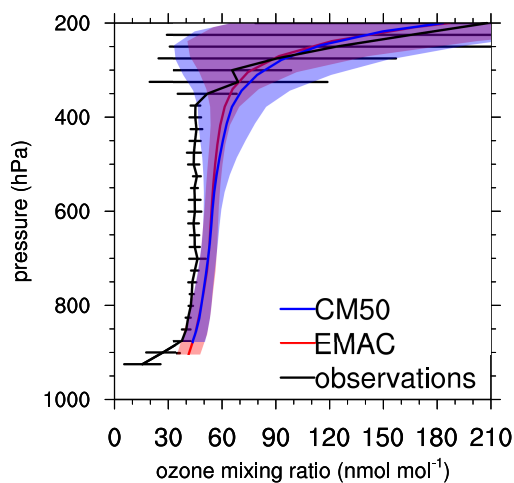


Figure S21: As Fig. S20 but for December 2008.

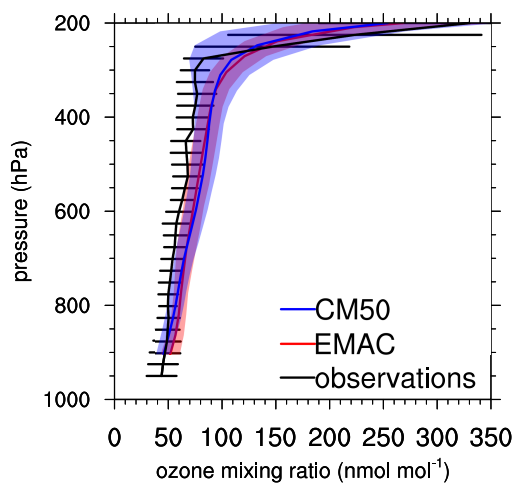


Figure S22: Vertical ozone profile at Payerne for June 2008. The standard deviation of the temporal mean is indicated by the error bars for the observations and by the shaded area for the model data.

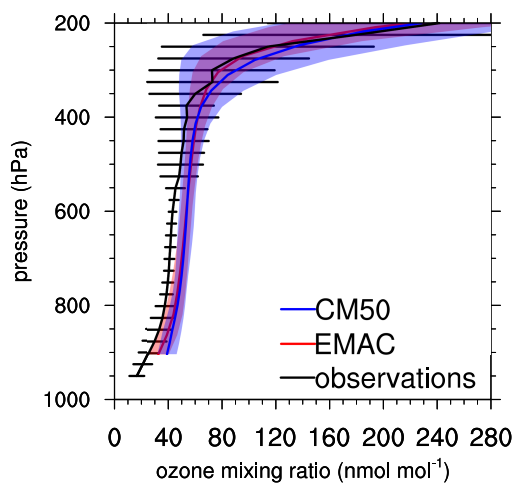


Figure S23: As Fig. S23 but for December 2008.

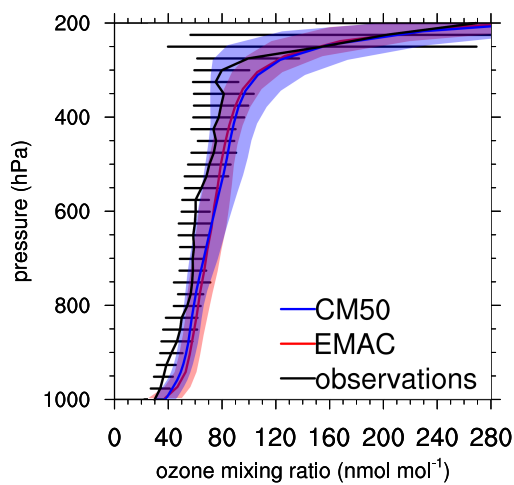


Figure S24: Vertical ozone profile at Uccle for June 2008. The standard deviation of the temporal mean is indicated by the error bars for the observations and by the shaded area for the model data.

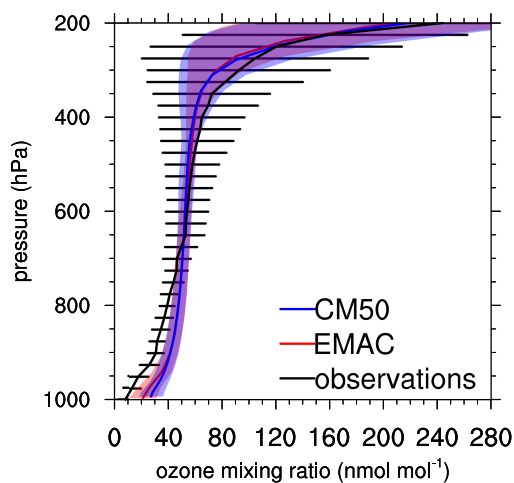


Figure S25: As Fig. S25 but for December 2008.

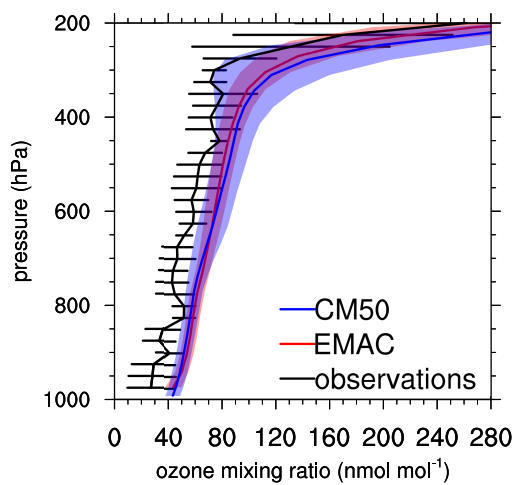


Figure S26: Vertical ozone profile at Legionowo for June 2008. The standard deviation of the temporal mean is indicated by the error bars for the observations and by the shaded area for the model data.

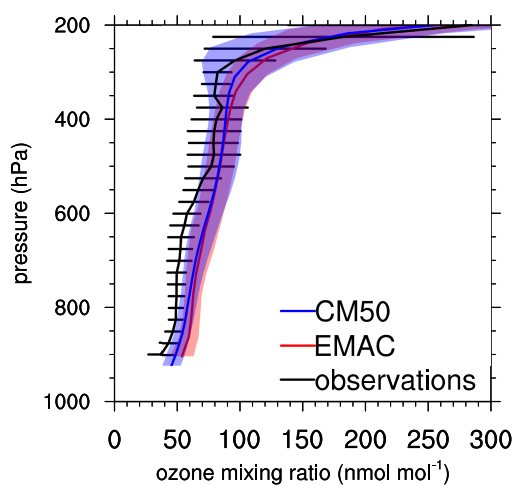


Figure S27: Vertical ozone profile at Hohenpeissenberg for June 2008. The standard deviation of the temporal mean is indicated by the error bars for the observations and by the shaded area for the model data.

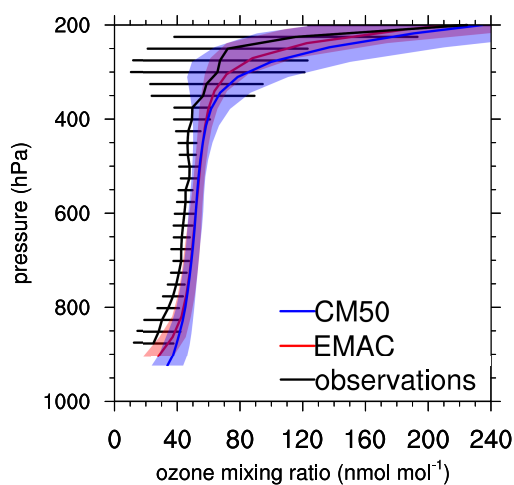


Figure S28: Vertical ozone profile at Hohenpeissenberg for June 2008. The standard deviation of the temporal mean is indicated by the error bars for the observations and by the shaded area for the model data.

S2 Comparison with ERA-Interim

S2.1 CM50

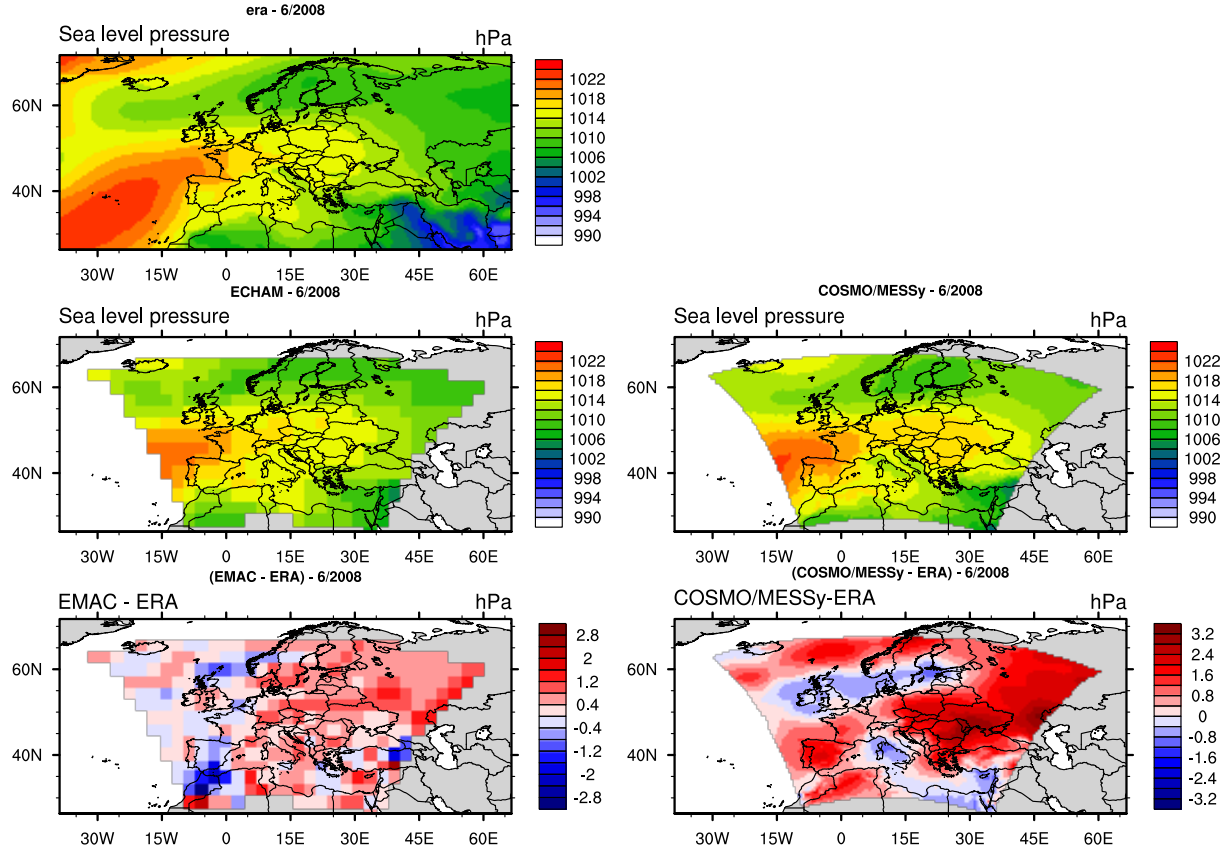


Figure S29: Comparison of the mean sea level pressure (in hPa) between EMAC, CM50 and ERA Interim for June 2008. The upper three plots show the absolute values for ERA-Interim, EMAC and CM50. The lower row depicts the difference to ERA-Interim for EMAC (left) and CM50 (right).

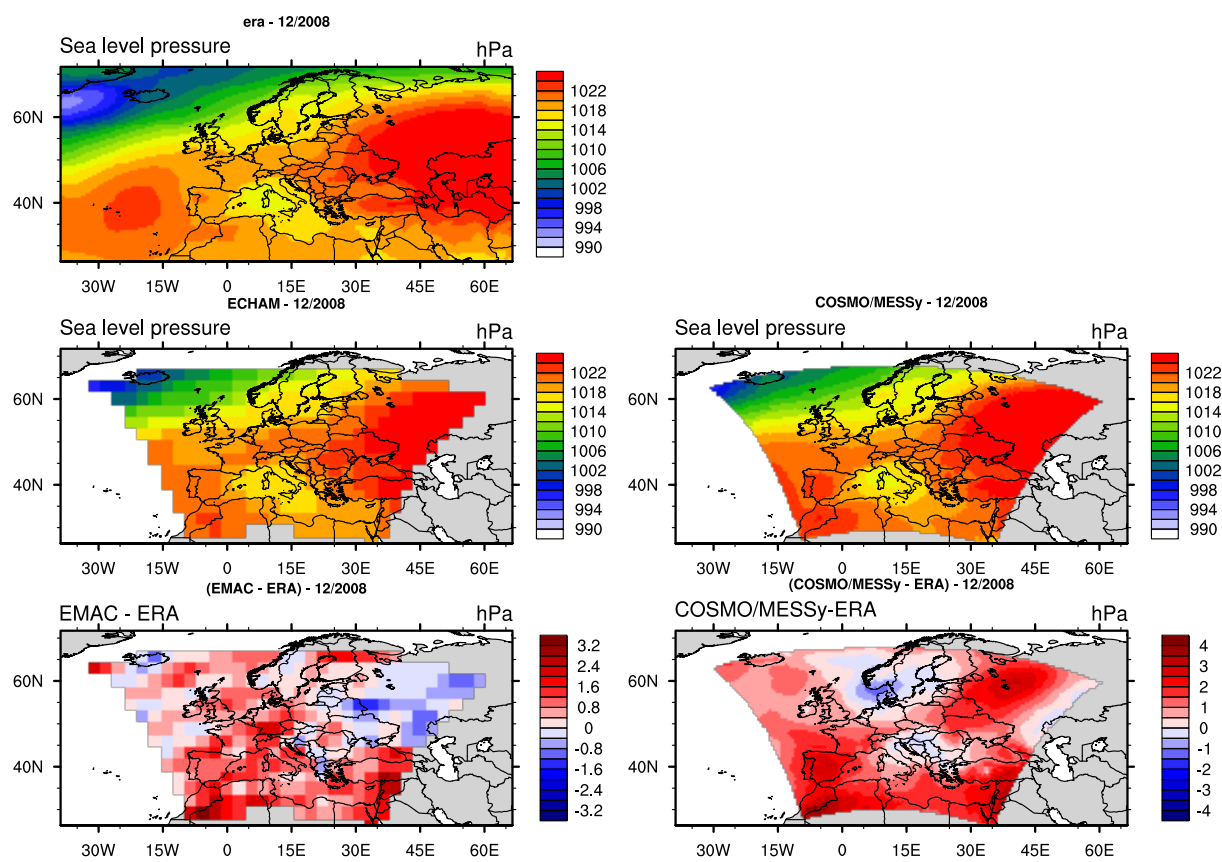


Figure S30: As Fig. S29 but for December 2008.

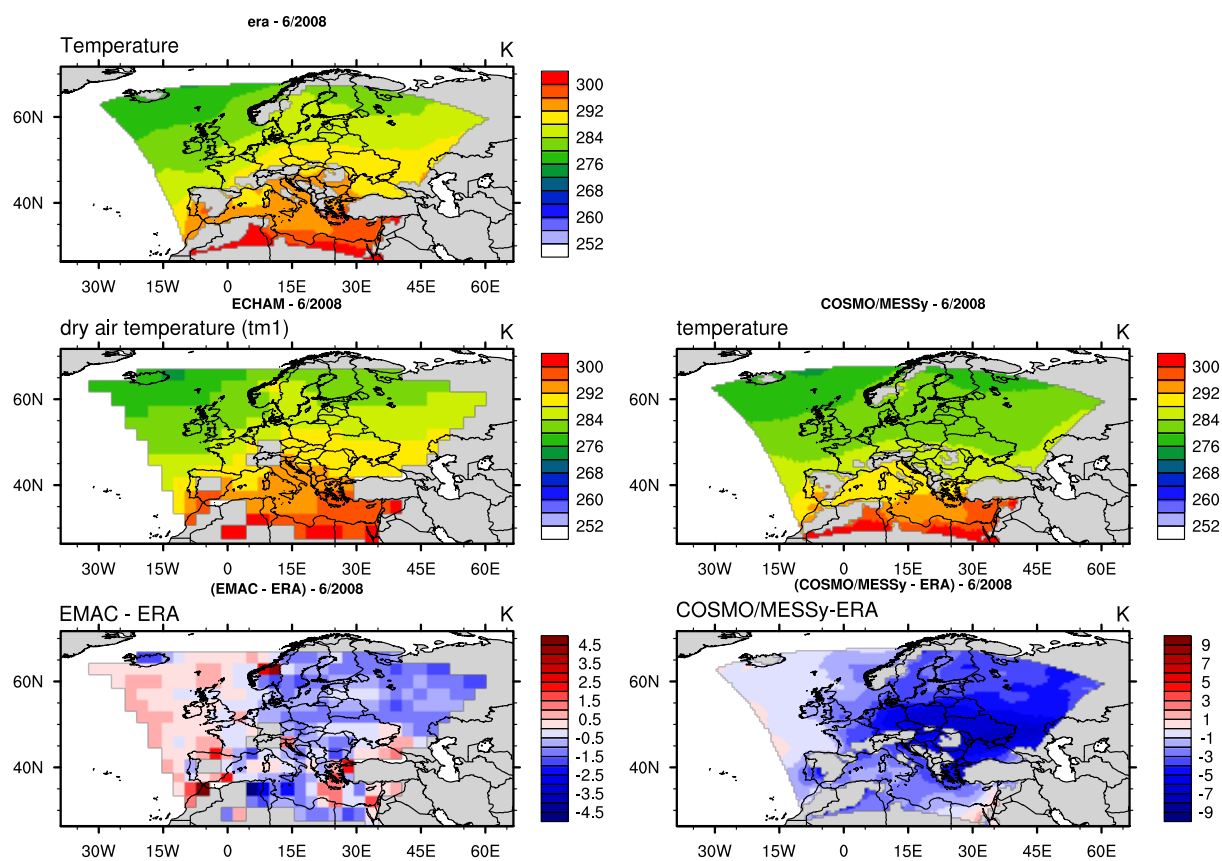


Figure S31: Comparison of the temperature at 950 hPa (in K) between EMAC, CM50 and ERA Interim for June 2008. The upper three plots show the absolute values for ERA-Interim, EMAC and CM50. The lower row depicts the difference to ERA-Interim for EMAC (left) and CM50 (right).

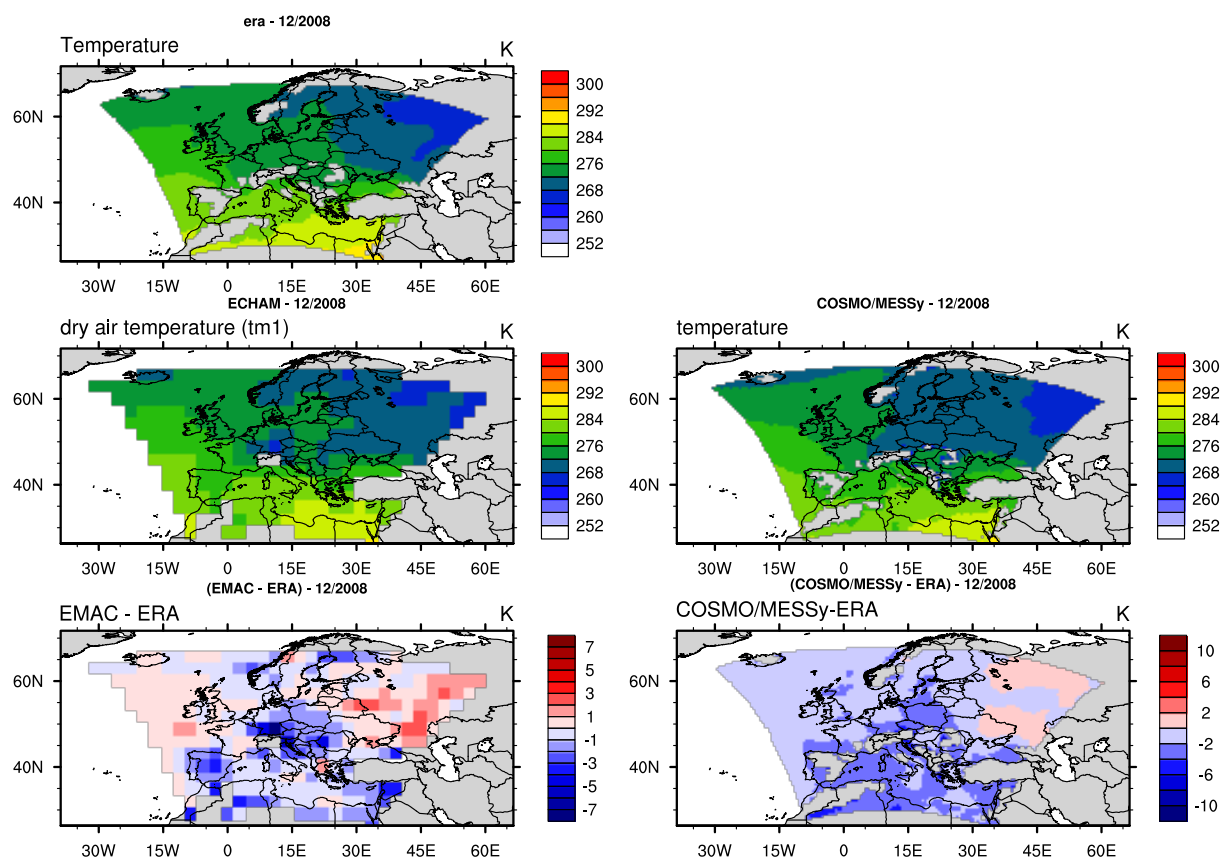


Figure S32: As Fig. S31 but for December 2008.

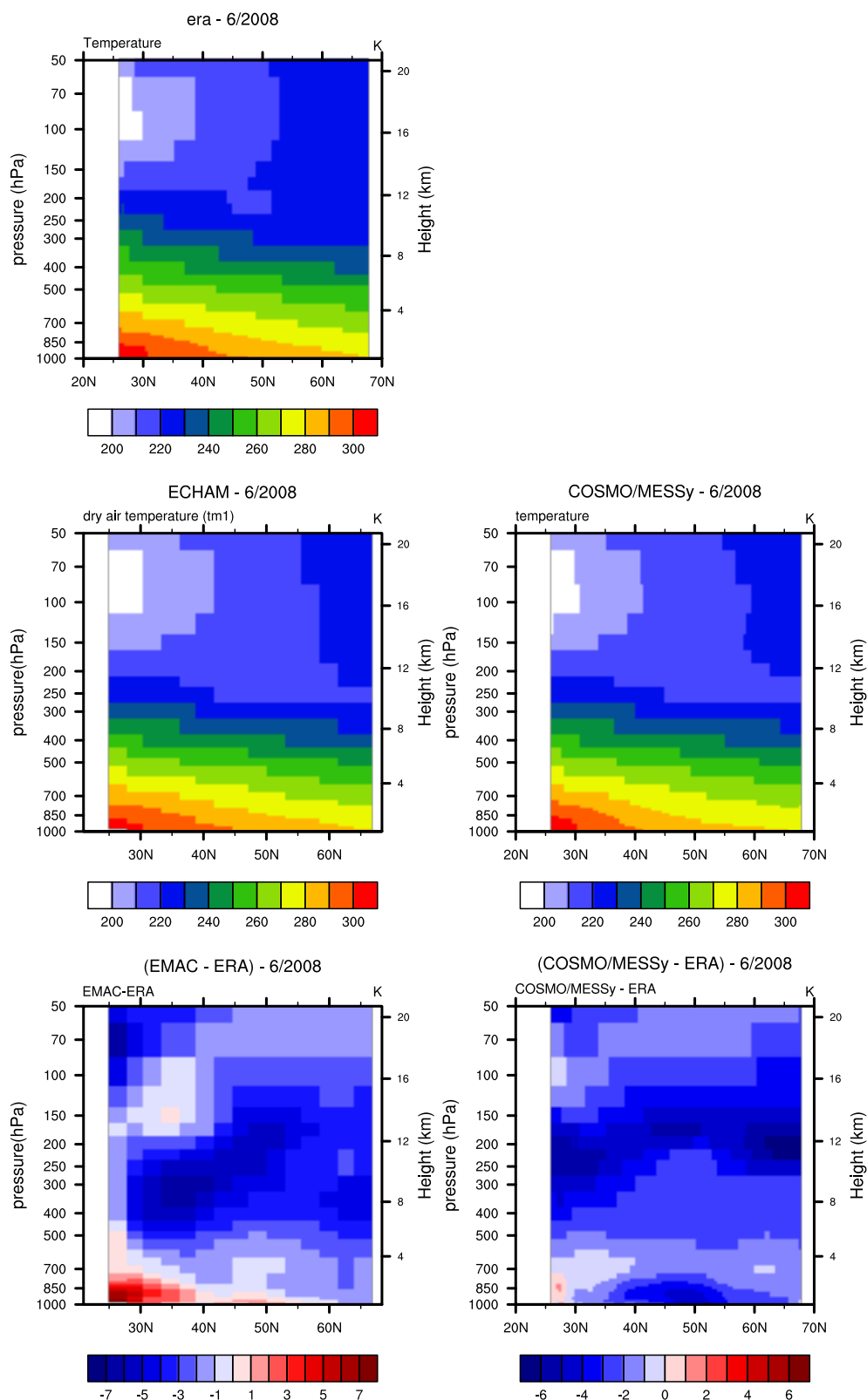


Figure S33: Comparison of the zonal average temperature (in K) between EMAC, CM50 and ERA Interim for June 2008. The upper three plots show the absolute values for ERA-Interim, EMAC and CM50. The lower row depicts the difference to ERA-Interim for EMAC (left) and CM50 (right).

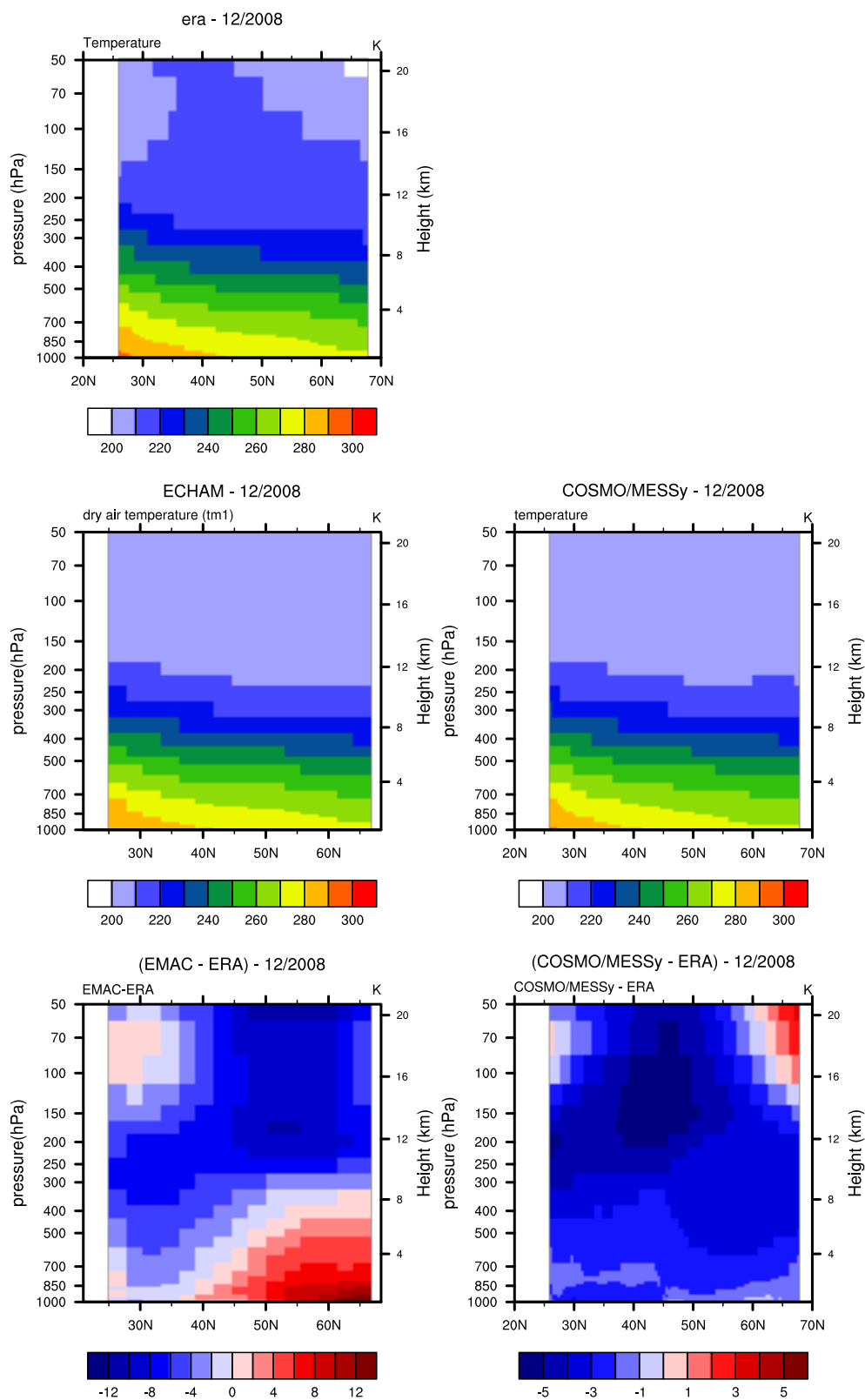


Figure S34: As Fig. S33 but for December 2008.

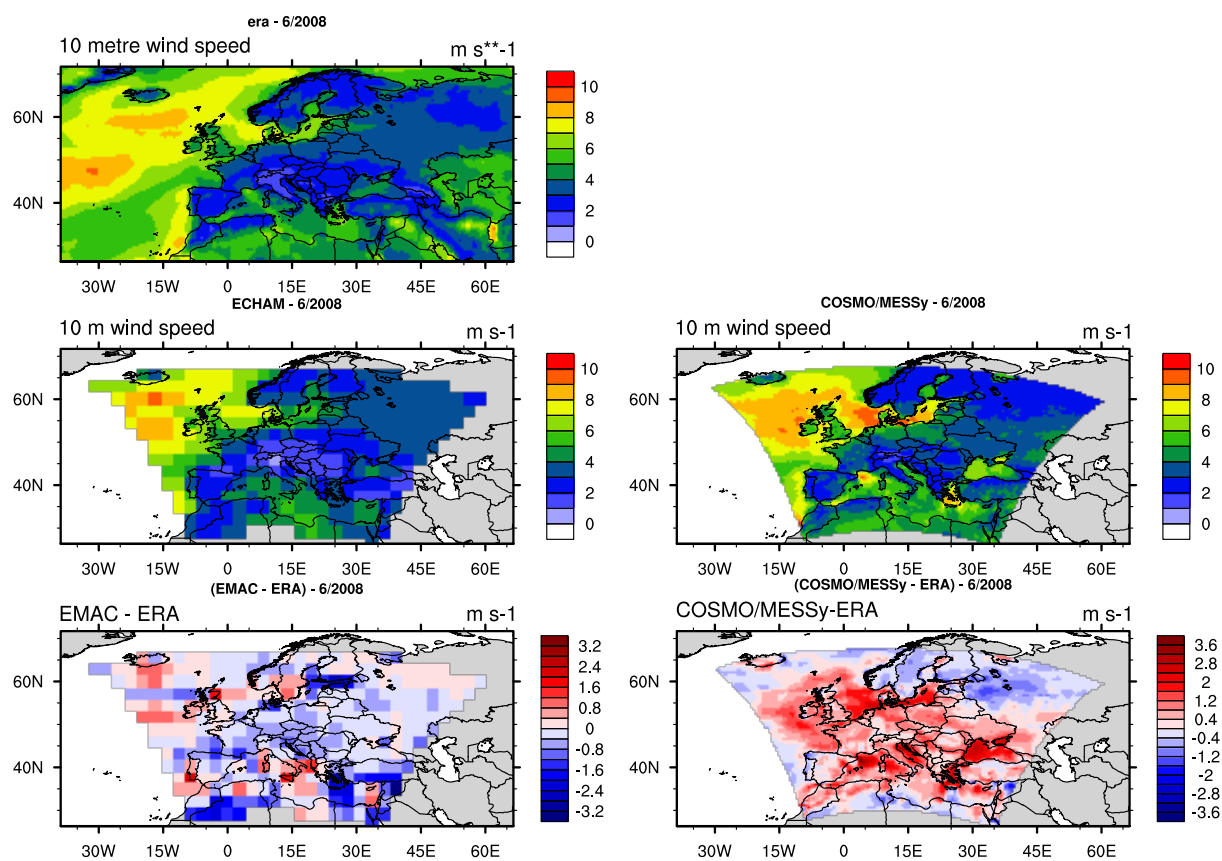


Figure S35: Comparison of the 10 meter wind speed (in m s^{-1}) between EMAC, CM50 and ERA Interim for June 2008. The upper three plots show the absolute values for ERA-Interim, EMAC and CM50. The lower row depicts the difference to ERA-Interim for EMAC (left) and CM50 (right).

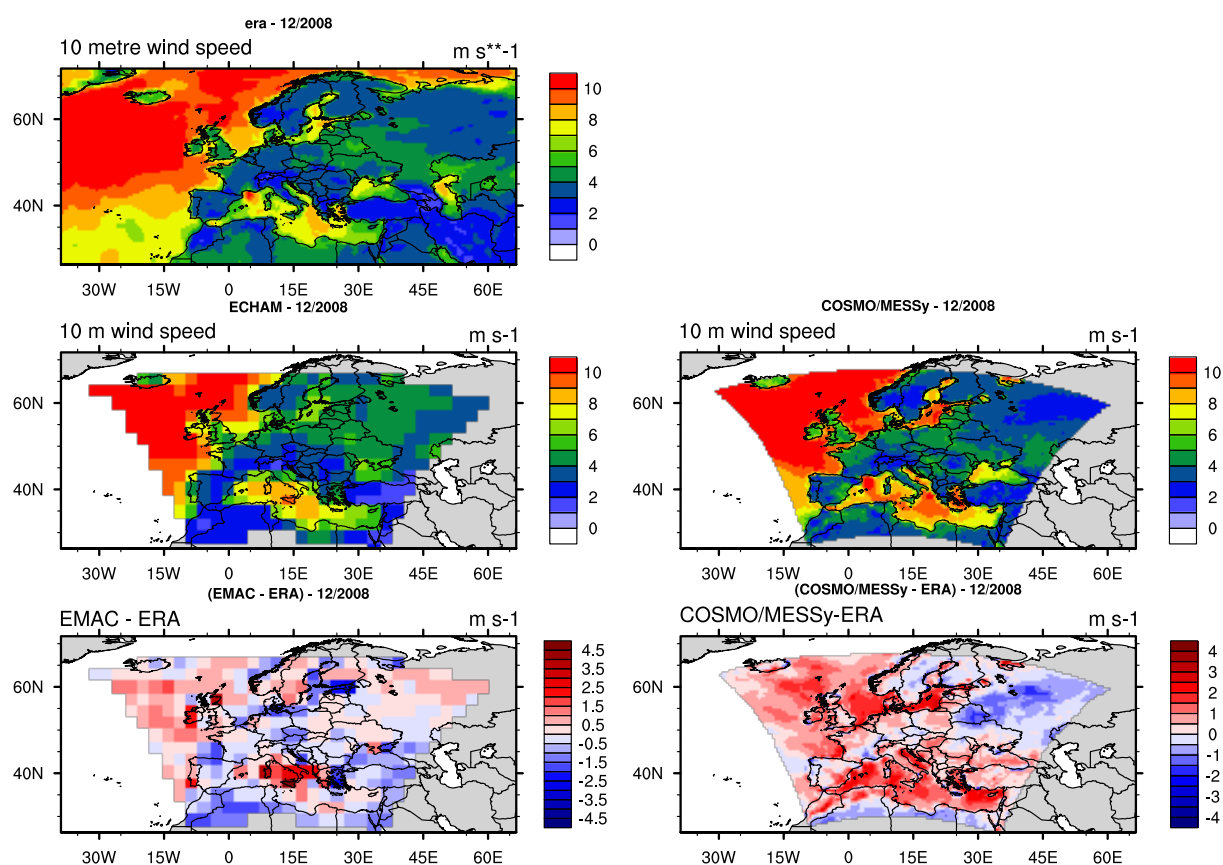


Figure S36: Comparison of the 10 meter wind speed (in m s^{-1}) between EMAC, CM50 and ERA Interim for December 2008. The upper three plots show the absolute values for ERA-Interim, EMAC and CM50. The lower row depicts the difference to ERA-Interim for EMAC (left) and CM50 (right).

S2.2 CM12

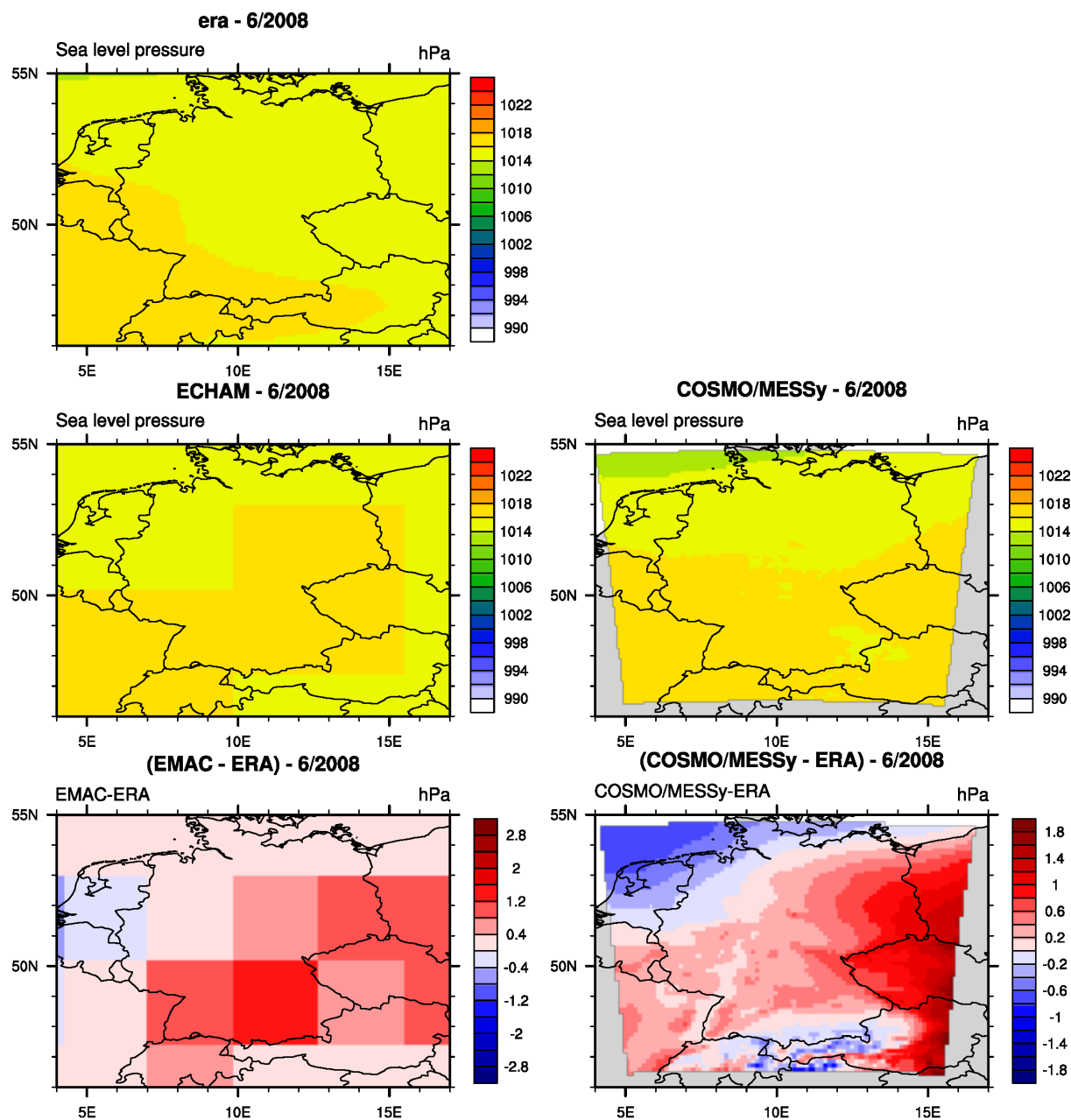


Figure S37: Comparison of the mean sea level pressure (in hPa) between EMAC, CM12 and ERA Interim for June 2008. The upper three plots show the absolute values for ERA-Interim, EMAC and CM12. The lower row depicts the difference to ERA-Interim for EMAC (left) and CM50 (right).

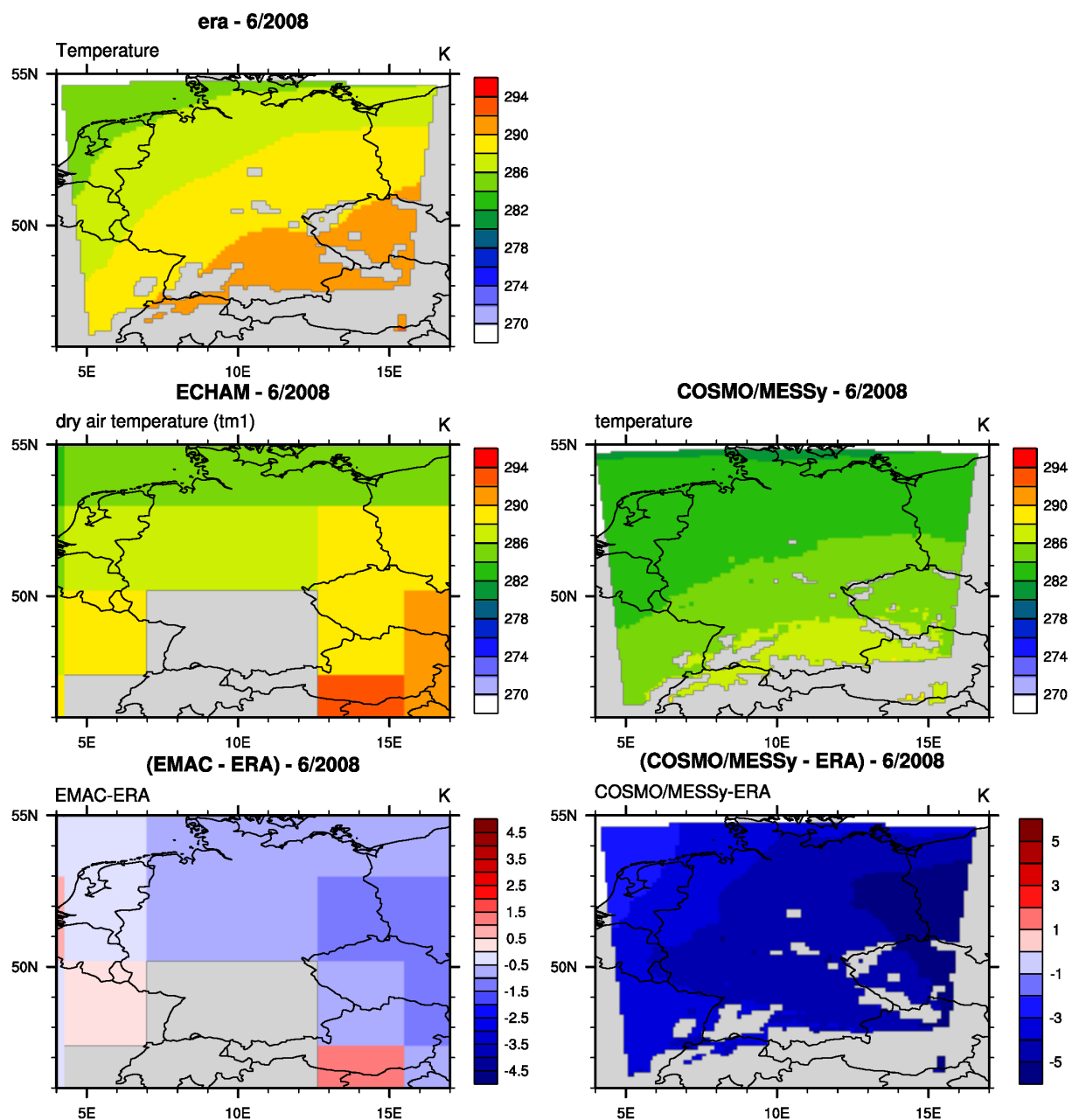


Figure S38: Comparison of the temperature at 950 hPa (in K) between EMAC, CM12 and ERA Interim for June 2008. The upper three plots show the absolute values for ERA-Interim, EMAC and CM12. The lower row depicts the difference to ERA-Interim for EMAC (left) and CM50 (right).

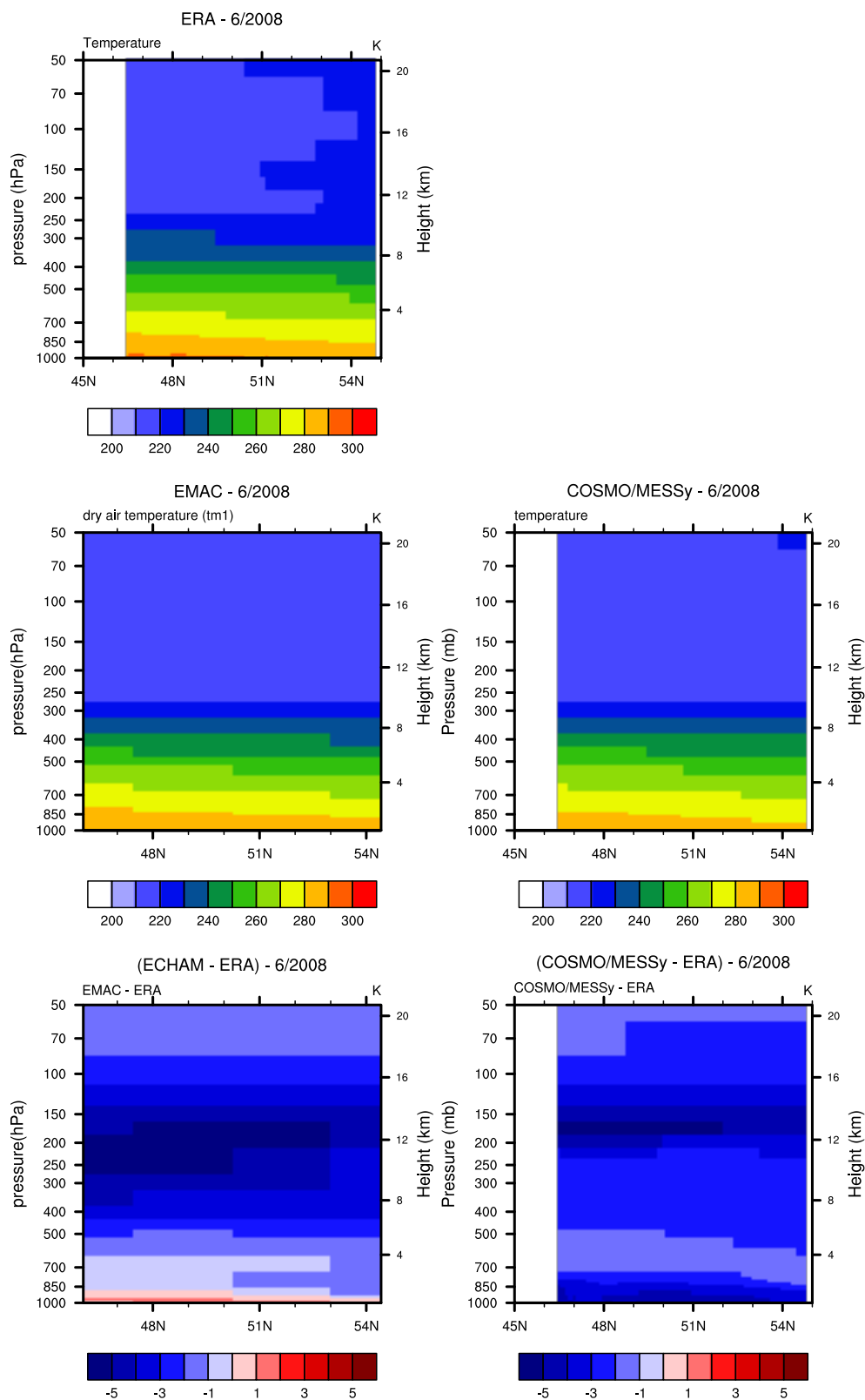


Figure S39: Comparison of zonal average temperature (in K) between EMAC, CM12 and ERA Interim for June 2008. The upper three plots show the absolute values for ERA-Interim, EMAC and CM12. The lower row depicts the difference to ERA-Interim for EMAC (left) and CM50 (right).

S3 Comparison with temperature profiles from ozone sondes

S3.1 CM50

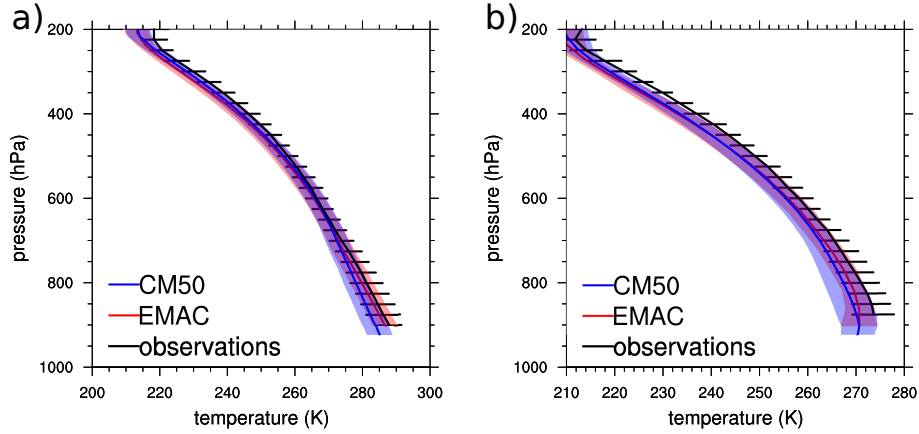


Figure S40: Vertical temperature profile at Hohenpeissenberg (in K) for **a)** June and **b)** December 2008. The standard deviation of the temporal mean is indicated by the error bars for the observations and by the shaded area for the model data.

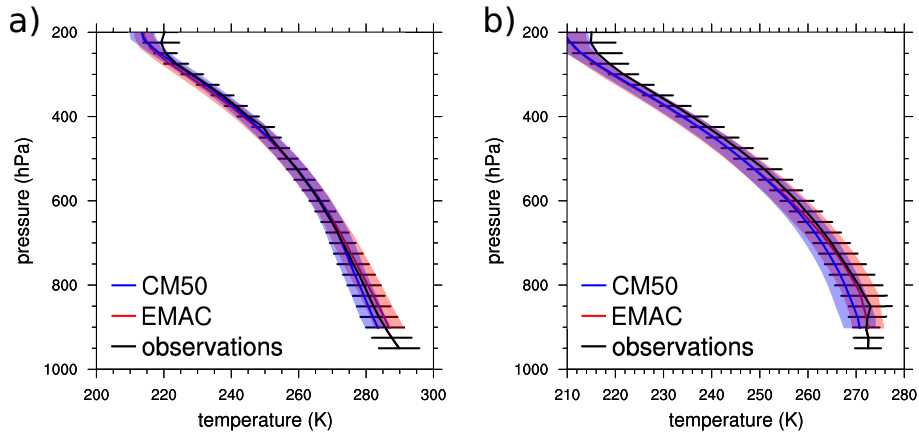


Figure S41: Vertical temperature profile at Payerne (in K) for (a) June and (b) December 2008. The standard deviation of the temporal mean is indicated by the error bars for the observations and by the shaded area for the model data.

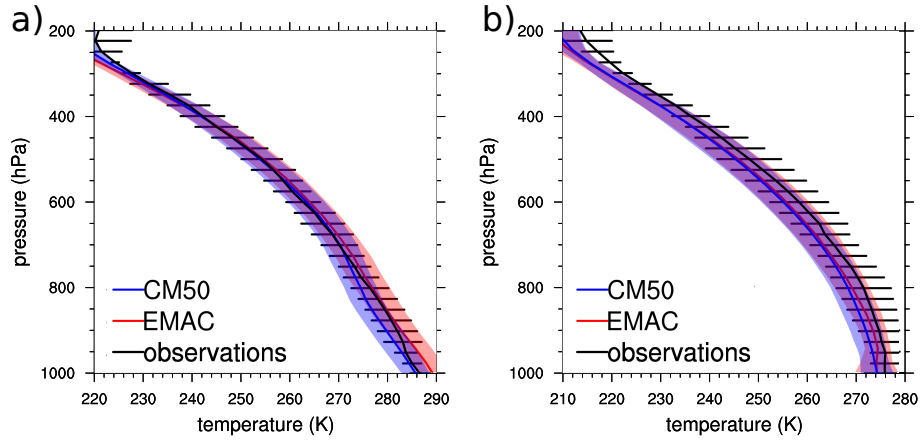


Figure S42: Vertical temperature profile at De Bilt (in K) for (a) June and (b) December 2008. The standard deviation of the temporal mean is indicated by the error bars for the observations and by the shaded area for the model data.

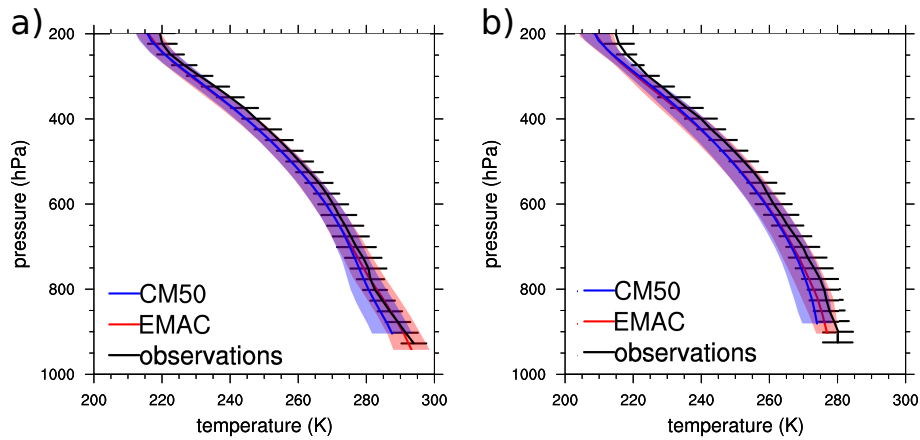


Figure S43: Vertical temperature profile at Madrid (in K) for (a) June and (b) December 2008. The standard deviation of the temporal mean is indicated by the error bars for the observations and by the shaded area for the model data.

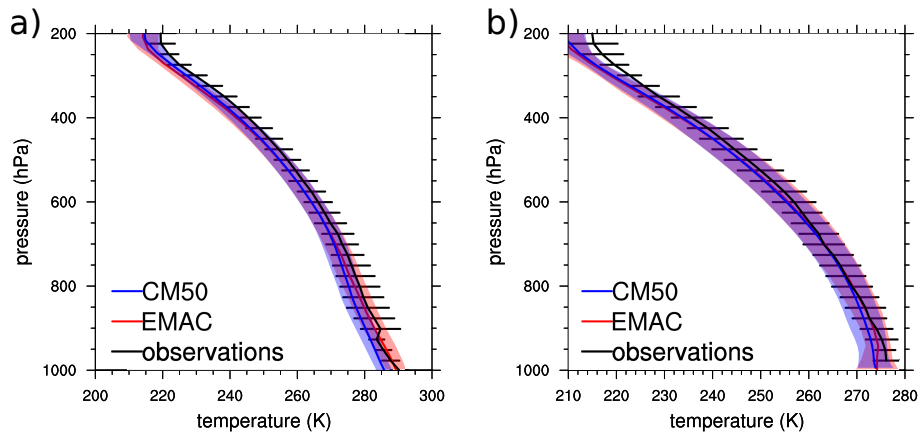


Figure S44: Vertical temperature profile at Uccle (in K) for (a) June and (b) December 2008. The standard deviation of the temporal mean is indicated by the error bars for the observations and by the shaded area for the model data.

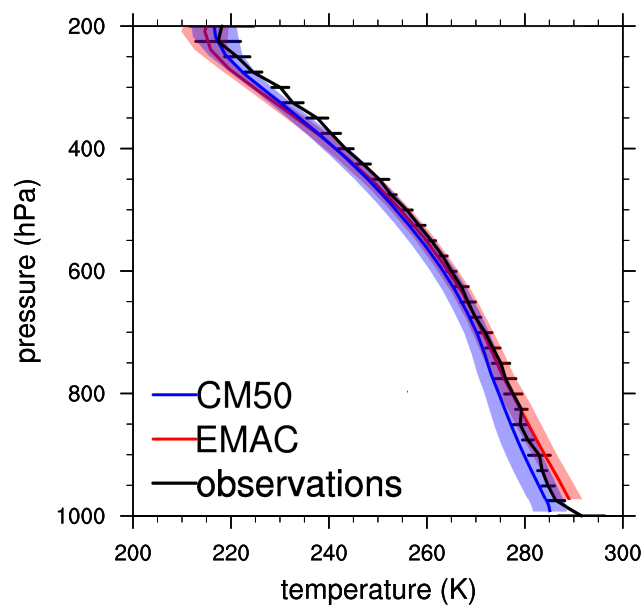


Figure S45: Vertical temperature profile at Legionowo for June 2008. The standard deviation of the temporal mean is indicated by the error bars for the observations and by the shaded area for the model data.

S4 COSMO-Namelist

The section shows a comparison between the COSMO namelists used in this study and the COSMO-CLM namelists for the simulations within the EURO CORDEX framework (Kotlarski et al., 2014). Please note that this study uses a newer version of COSMO-CLM compared to the simulations described by Kotlarski et al. (2014), therefore some new namelist options are now available or defaults have been changed.

S4.1 'lmgrid'-namelist

Table S1: Comparison between the COSMO-lmgrid namelist used in this study and the CORDEX-EU COSMO-CLM namelist (please note that the namelist for CORDEX-EU is from the COSMO-CLM version 4.8-clm17, while we use COSMO 5.0, therefore some options are not available in COSMO 4.8-clm17 (marked with *)).

Variable	CM50	CM12	CORDEX-EU
pollon	-170	-170	-162
pollat	40	41	39.25
polgam	0	0	0
dlon	0.44	0.1	0.44
dlat	0.44	0.1	0.44
startlon_tot	-3.9	-25.6	-33.93
startlat_tot	-4.9	-27.6	-28.93
ie_tot	132	104	132
je_tot	122	114	129
ke_tot	40	40	40

S4.2 'runctl'-namelist

Table S2: Comparison between the COSMO-runcontrol namelist used in this study and the CORDEX-EU COSMO-CLM namelist (please note that the namelist for CORDEX-EU is from the COSMO-CLM version 4.8-clm17, while we use COSMO 5.0, therefore some options are not available (marked with *)).

Variable	CM50	CM12	CORDEX-EU
dt	240	120	300
itype_calendar	0	0	0
hincmxt	6	6	24
hincmxu	1	1	24
leps	F	F	F
lphys	T	T	T
ldiagnos	T	T	T
ldfi	F	F	F
luseobs	F	F	F
luse_rtov	F	F	F
lcosmo_art	F	F	*
lpollen	F	F	*
ldump_ascii	T	T	F
lreproduce	T	T	T
lreorder	F	F	F
lartif_data	F	F	F
lperi_x	F	F	*
lperi_y	F	F	*
l2dim	F	F	F
lroutine	F	F	*
llm	F	F	F
nprocx	12	20	16
nprocy	16	16	16
nprocio	0	0	0
num_asyncio_comm	0	0	*
num_iope_percomm	0	0	*
nboundlines	3	3	3
ncomm_type	1	1	3
ldatatypes	F	F	F
ltime_barrier	T	T	F
itype_timing	4	4	4
idbg_level	10	10	2
ldebug_dyn	F	F	F
ldebug_gsp	F	F	F
ldebug_rad	F	F	F
ldebug_tur	F	F	F
ldebug_con	F	F	F
ldebug_soi	F	F	F
ldebug_io	F	F	F
ldebug_mpe	F	F	F
ldebug_dia	F	F	F
ldebug_art	F	F	F
ldebug_ass	F	F	F
ldebug_lhn	F	F	F

Continued on next page

Table S2 – *Continued from previous page*

Variable	CM50	CM12	CORDEX-EU
lprintdeb_all	F	F	F
linit_fields	F	F	F

S4.3 'tuning'-namelist

Table S3: Comparison between the COSMO-tuning namelist used in this study and the CORDEX-EU COSMO-CLM namelist (please note that the namelist for CORDEX-EU is from the COSMO-CLM version 4.8 -clm17, while we use COSMO 5.0, therefore some options are not available (marked with *)).

Variable	CM50	CM12	CORDEX-EU
crsmin	150	150	150
rat_lam	1	1	1
tkesmot	0.15	0.15	0.15
wichfakt	0.15	0.15	0
securi	0.5	0.5	0.85
tkhmin	1	1	1
tkmmin	1	1	1
rlam_mom	0	0	0
rlam_heat	1	1	1
rat_sea	20	20	20
rat_can	1	1	1
c_lnd	2	2	2
c_sea	1.5	1.5	1.5
c_soil	1	1	1
e_surf	1	1	1
pat_len	500	500	500
tur_len	500	500	500
z0m_dia	0.2	0.2	0.2
a_heat	0.74	0.74	0.74
a_mom	0.92	0.92	0.92
d_heat	10.1	10.1	10.1
d_mom	16.6	16.6	16.6
c_diff	0.2	0.2	0.2
a_hshr	0.2	0.2	*
a_stab	0	0	*
clc_diag	0.5	0.5	0.5
q_crit	4	4	4
qc0	0	0	0
qi0	0	0	0
gkdrag	0.075	0.075	0.075
gkwake	0.5	0.5	0.5
mu_rain	0	0.5	0.5
rain_n0_factor	1	1	*
v0snow	25	25	25
cloud_num	500000000	500000000	500000000
entr_sc	0.0003	0.0003	0.0003
thick_sc	25000	25000	*

S4.4 'dyncontrol'-namelist

Table S4: Comparison between the COSMO-dyncontrol namelist used in this study and the CORDEX-EU COSMO-CLM namelist (please note that the namelist for CORDEX-EU is from the COSMO-CLM version 4.8-clm17, while we use COSMO 5.0, therefore some options are not available (marked with *)).

Variable	CM50	CM12	CORDEX-EU
epsass	0.15	0.15	0.15
alphaass	1	1	0.53
betasw	0.4	0.4	0.4
betagw	0.4	0.4	0.4
beta2sw	0.4	0.4	0.4
beta2gw	0.4	0.4	0.4
lrubc	F	F	F
lspubc	T	T	T
lexpl_lbc	T	T	T
lradlbc	F	F	F
lcond	T	T	T
ldiabf_lh	T	T	T
lw_freeslip	T	T	T
l2tls	T	T	T
y_vert_adv_dyn	impl2	impl2	*
lsemi_imp	F	F	F
lhordiff	T	T	*
ldyn_bbc	F	F	T
lcori	T	T	T
lmetr	T	T	T
lcori_deep	F	F	F
ladv_deep	F	F	F
y_scalar_advect	BOTT2	BOTT2	BOTT2
rdheight	11000	11000	11000
crltau	1	1	1
rlwidth	700000	150000	500000
relax_fac	0.01	0.01	0.01
nrddtau	6	6	6
maxit_si	200	200	200
ikrylow_si	20	20	20
iprint_si	0	0	0
irunge_kutta	1	1	1
irk_order	3	3	3
iadv_order	5	5	3
ieva_order	3	3	3
itheta_adv	0	0	0
ltadv_limiter	F	F	*
itype_bbc_w	1	1	*
inter_max	1	1	1
itype_outflow_qrsg	1	1	1
itype_lbc_qrsg	1	1	1
itype_spubc	1	1	1
nfi_spubc2	10	10	10
itype_hdiff	2	2	2

Continued on next page

Table S4 – *Continued from previous page*

Variable	CM50	CM12	CORDEX-EU
l_diff_Smag	T	T	*
hd_corr_u_bd	0	0	0.25
hd_corr_t_bd	0	0	*
hd_corr_trcr_bd	0	0	*
hd_corr_p_bd	0	0	*
hd_corr_u_in	0	0	*
hd_corr_t_in	0	0	*
hd_corr_trcr_in	0	0	*
hd_corr_p_in	0	0	*
hd_dhmax	250	250	250
xkd	0.1	0.1	0.1
divdamp_slope	20	20	*
eps_si	0	0	0
itype_fast_waves	1	1	*
lspecnudge	F	F	F

S4.5 'phycontrol'-namelist

Table S5: Comparison between the COSMO-phycontrol namelist used in this study and the CORDEX-EU COSMO-CLM namelist (please note that the namelist for CORDEX-EU is from the COSMO-CLM version 4.8 -clm17, while we use COSMO 5.0, therefore some options are not available (marked with *)).

Variable	CM50	CM12	CORDEX-EU
lgsp	T	T	T
ldiniprec	T	T	F
lrad	T	T	T
itype_aerosol	1	1	*
lemiss	F	F	*
lforest	F	F	T
ltur	T	T	T
l3dturb	F	F	F
l3dturb_metr	T	T	T
lprog_tke	F	F	F
limpltkediff	T	T	*
lconv	T	T	T
itype_conv	0	0	0
lconv_inst	F	F	F
lsoil	T	T	T
lseaiice	F	F	*
llake	F	F	F
lso	T	T	T
lmelt	T	T	T
lmelt_var	T	T	T
lmulti_layer	T	T	T
ke_soil	7	7	9
czbot_w_so	4	4	9
lturhor	F	F	F
lexpcor	F	F	F
ltmpcor	F	F	F
lprfcor	F	F	F
lnonloc	F	F	F
lcpfluc	F	F	F
lconf_avg	T	T	T
lradf_avg	F	F	F
lcape	F	F	F
lctke	F	F	F
hincrad	1	1	1
3 nincrad	12	12	12
nradcoarse	1	1	1
ninctura	1	1	1
nincconv	1	1	1
nincsso	5	5	5
itype_trvg	2	2	2
itype_evsl	2	2	2
itype_gscp	3	3	
itype_weld	2	2	2
itype_tran	2	2	2

Continued on next page

Table S5 – *Continued from previous page*

Variable	CM50	CM12	CORDEX-EU
itype_turb	3	3	3
itype_synd	2	2	2
imode_tran	1	1	1
imode_turb	1	1	1
ico2_rad	8	8	8
iy_co2_stab	2001	2001	2001
lco2_stab	F	F	F
icldm_rad	4	4	4
icldm_tran	0	0	0
icldm_turb	2	2	2
nlgw	2	2	2
lrادتopo	F	F	F
nhorl	24	24	24
itype_albedo	2	2	2

S5 List of used stations

Table S6: Overview of stations from the EMEP network used for the comparison. Columns four to six indicate the height of the geometric height of the station as well as the height were the data are sample in COSMO and EMAC ('height corrected'). The '-' indicates that no height correction is performed. The last column shows for which variables the station data were used.

Name	lat (in °)	lon (in °)	h. station (in m)	h. COSMO (in m)	h. EMAC (in m)	variable
Aliartos	38.37	23.08	110	325	198	O3, NO2
Anholt	56.71	11.51	40	36	151	NO2
Aston Hill	52.50	-3.03	370	382	464	NO2
Auchencorth	55.79	-3.24	260	-	-	HNO3
Moss						
Ayia Marina	35.04	33.06	532	577	475	O3
Barcorotta	38.48	-6.92	393	376	362	O3, NO2
Birkesens	58.38	8.25	190	304	139	O3,NO2, HNO3
Cabau	51.97	4.93	1	12	3	NO2
Ziideweg						
Campisabalos	41.28	-3.14	1360	-	-	C5H8
Chopok	48.93	19.58	2008	2109	2108	NO2, HNO3
Dezi	52.30	4.50	4	10	84	NO2
Diabla Gora	54.15	22.07	157	-	-	HNO3
Els Torms	41.40	0.72	470	488	441	NO2
Eskdalemuir	51.57	-3.20	243	253	298	NO2
Eupen	50.63	6.00	295	311	201	O3, NO2
Forsthof	48.11	15.92	581	567	655	O3
Giordon	36.07	14.22	167	181	226	O3
Lighthouse						
Graz Platte	47.11	15.47	651	696	746	O3
Harwell	51.57	-13.16	137	136	144	NO2
Hoburgen	56.91	18.15	58	70	64	NO2
Hurdal	60.37	11.08	300	-	-	HNO3
Illmitz	47.76	16.76	117	204	329	CO,NO2,HNO3
Iskraba	45.57	14.87	520	520	575	O3,NO2
Ispira	45.80	8.63	209	1262	892	O3,NO2
Jarczew	51.82	21.98	180	180	233	O3,NO2
Jungfrau-joch	46.54	7.98	3578	3528	3581	O3,CO, NO2
Keldsnor	54.73	10.73	10	23	78	NO2
Kollumerwaard	53.33	6.28	1	11	-51	CO
Kosetice	49.58	15.08	535	519		NO2,CO,C5H8
Krvavec	46.30	14.54	1740	1736	1916	CO,HNO3
La Coulande	48.63	-0.45	304	333	323	O3
La Tardiere	46.65	-0.75	133	133	192	NO2
Ladybower	53.40	-1.75	420	358	503	O3,NO2
Research						
Lahemaa	59.50	25.90	32	56	17	O3
Lazaropole	41.54	20.69	1332	1351	1398	O3
Le Casset	45.00	6.47	1790	1736	1623	O3
Leova II	46.48	28.28	166	-	-	HNO3
Lullington	50.79	0.18	120	117	62	O3,NO2
Heathrow						

Continued on next page

Table S6 – *Continued from previous page*

Name	lat (in °)	lon (in °)	h. station (in m)	h. COSMO (in m)	h. EMAC (in m)	variable
Mace Head	53.17	-9.50	15	56	162	O3
Montellipreti	42.10	12.63	48	310	440	O3,NO2, HNO3
Narberth	51.78	-4.69	160	158	156	NO2
Neuglobsow	53.17	13.03	62	65	93	O3,NO2, HNO3, C5H8
Niembro	43.44	-4.85	134	468	532	O3, NO2
Noraa-Kvill	57.82	15.57	261	256	180	O3
O Savinao	43.23	-7.70	506	556	406	NO2
St. Osyth	51.78	1.08	8	32	62	CO,NO2
Pallas	68.0	24.15	340	-	-	C5H8
Penausende	41.28	-5.87	985	977	940	NO2
Peyrusse	43.62	0.19	200	379	500	C5H8, NO2
Vieille						
Pic du Midi	42.94	0.14	2887	2889	2736	O3
Preila	55.35	21.06	5	26	97	O3,NO2
Puy de Dome	45.77	2.95	1468	1486	1362	O3,CO
Revin	49.90	4.63	390	386	442	O3, HNO3
Rigi	47.07	8.46	1031	-	-	HNO3, C5H8
Rojen Peak	41.70	24.74	1750	1756	1724	O3
Rucava	56.16	21.17	18	46	114	O3
Schauinsland	47.92	7.92	1205	1258	1273	O3,CO, NO2, HNO3, C5H8
Schmücke	50.65	10.77	937	873	888	O3, NO2, C5H8
Søgne	58.11	7.85	15	-	-	HNO3
Sniezka	50.73	15.73	1603	1521	1507	NO2
Sonnblick	47.05	12.96	3106	3099	3301	CO
Starina	49.05	22.27	345	491	446	O3,NO2, HNO3, C5H8
Sulzberg	47.53	9.93	1020	1067	1001	O3
Svratouch	49.83	16.05	737	727	685	NO2
La Tardiäre	46.65	-0.75	133	-	-	C5H8
Tustervatn	65.83	13.91	439	-	-	HNO3
Ulborg	56.28	8.43	10	31	139	O3
Vilsandi	58.38	21.81	6	12	114	O3
Vizna	37.23	-3.53	1296	1209	1103	O3, NO2
Vorhegg	46.62	12.97	1020	1192	902	CO,NO2
Vredepel	51.54	5.85	28	32	84	NO2
Waldhof	52.80	10.75	74	77	278	O3, NO2, HNO3, C5H8
Westerland	54.93	8.31	12	15	12	O3, NO2, HNO3
Zarra	39.09	-1.10	885	840	984	NO2
Zingst	54.43	12.73	1	11	93	O3, NO2, HNO3, O3, NO2, C5H8,
Zoesni	57.14	25.91	188	200	173	HNO3 O3, NO2, C5H8

Table S7: Overview of stations providing vertical ozone profiles used for comparison. The last column shows for which variables the station data were used.

Name	lat (in °)	lon (in °)	height (in m)	variable
De Bilt	52.10	5.18 E	2	O3
Hohenpeißenberg	47.80	11.01	985	O3, C5H8
Leginowo	52.40	29.97	96	O3
Madrid	40.45	3.72	680	O3
Payerne	46.81	6.94	490	O3
Uccle	50.80	4.36	100	O3
Valentia	51.94	10.25	14	O3

S6 Detailed list of used submodels

Table S8: Overview of the submodels running in EMAC and COSMO/MESSy respectively. Both COSMO/MESSy instances use the same submodels.

Submodel	EMAC	COSMO	short description	references
AEROPT	x		calculation of aerosol optical properties	Dietmüller et al. (2016)
AIRSEA	x	x	exchange of tracers between air and sea	Pozzer et al. (2006)
CH4	x		methane oxidation and feedback to hydrological cycle	
CLOUD	x		cloud parametrisation	Roeckner et al. (2006), Jöckel et al. (2006)
CLOUDOPT	x		cloud optical properties	
CONVECT	x		convection parametrisation	Tost et al. (2006b)
CVTRANS	x	x	convective tracer transport	Tost et al. (2010)
DRADON	x	x	emission and decay of ²²² Radon	Jöckel et al. (2010)
DDEP	x	x	dry deposition of aerosols and tracer	Kerkweg et al. (2006a)
E2COSMO	x		additional ECHAM5 fields for COSMO coupling	Kerkweg and Jöckel (2012)
GWAVE	x		parametrisation of non-orographic gravity waves	Roeckner et al. (2003)
H2O	x		stratospheric water vapour and its feedback	Jöckel et al. (2006)
JVAL	x	x	calculation of photolysis rates	Landgraf and Crutzen (1998), Jöckel et al. (2006)
LNOX	x		NO _x -production by lighting	Tost et al. (2007), Jöckel et al. (2010)
MECCA	x	x	tropospheric and stratospheric gas-phase chemistry	Sander et al. (2011), Jöckel et al. (2010)
MMD*	x	x	coupling of EMAC and COSMO/MESSy (including libraries and all submodels)	Kerkweg and Jöckel (2012)
MSBM	x	x	multiphase chemistry of the stratosphere	Jöckel et al. (2010)
O3ORIG	x		ozone origin diagnostics	Grewe (2006)
OFFEMIS	x	x	prescribed emissions of trace gases and aerosols	Kerkweg et al. (2006b)
ONEMIS	x	x	on-line calculated emissions of trace gases and aerosols	Kerkweg et al. (2006b)
ORBIT	x	x	Earth orbit calculations	Dietmüller et al. (2016)
PTRAC	x	x	definition of prognostic tracers	Jöckel et al. (2008)
QBO	x		Newtonian relaxation of the quasi-biennial oscillation (QBO)	Giorgetta and Bengtsson (1999), Jöckel et al. (2006)
RAD	x		radiative transfer calculations calculation	Dietmüller et al. (2016)
S4D	x	x	diagnostic sampling along predefined tracks	Jöckel et al. (2010)
SATSIMS	x		satellite simulator	
SCALC	x	x	simple calculations	Jöckel et al. (2010)
SCAV	x	x	wet deposition and scavenging of trace gases and aerosols	Tost et al. (2006a)
SCOUT	x	x	diagnostic sampling at predefined locations	Jöckel et al. (2010)
SEDI	x	x	sedimentation of aerosols	Kerkweg et al. (2006a)
SORBIT	x	x	sampling along sun synchronous satellite orbits	Jöckel et al. (2010)

Continued on next page

Table S8 – *Continued from previous page*

Submodel	EMAC	COSMO	short description	references
SURFACE	x		surface properties	Jöckel et al. (2016)
TAGGING	x	x	TAGGING of source attributions	Grewe et al. (2016)
TBUDGET	x		contribution of processes to a tracer	Jöckel et al. (2016)
TNUDGE	x	x	Newtonian relaxation of tracers	Kerkweg et al. (2006b)
TREXP	x		emission of tracers at point sources	Jöckel et al. (2010)
TROPOP	x	x	diagnostic calculation of tropopause height and additional diagnostics	Jöckel et al. (2006)
VISO	x	x	sampling on isosurfaces	Jöckel et al. (2010)

S7 References

References

- Dietmüller, S., Jöckel, P., Tost, H., Kunze, M., Gellhorn, C., Brinkop, S., Frömming, C., Ponater, M., Steil, B., Lauer, A., and Hendricks, J.: A new radiation infrastructure for the Modular Earth Submodel System (MESSy, based on version 2.51), *Geoscientific Model Development*, 9, 2209–2222, doi:10.5194/gmd-9-2209-2016, URL <http://www.geosci-model-dev.net/9/2209/2016/>, 2016.
- Giorgetta, M. A. and Bengtsson, L.: Potential role of the quasi-biennial oscillation in the stratosphere-troposphere exchange as found in water vapor in general circulation model experiments, *J. Geophys. Res. Atmos.*, 104, 6003–6019, doi:10.1029/1998JD200112, URL <http://dx.doi.org/10.1029/1998JD200112>, 1999.
- Grewe, V.: The origin of ozone, *Atmos. Chem. Phys.*, 6, 1495–1511, doi:10.5194/acp-6-1495-2006, URL <http://www.atmos-chem-phys.net/6/1495/2006/>, 2006.
- Grewe et al.: Manuscript in preparation for GMD(D), 2016.
- Jöckel, P., Tost, H., Pozzer, A., Brühl, C., Buchholz, J., Ganzeveld, L., Hoor, P., Kerkweg, A., Lawrence, M., Sander, R., Steil, B., Stiller, G., Tanarhte, M., Taraborrelli, D., van Aardenne, J., and Lelieveld, J.: The atmospheric chemistry general circulation model ECHAM5/MESSy1: consistent simulation of ozone from the surface to the mesosphere, *Atmos. Chem. Phys.*, 6, 5067–5104, doi:10.5194/acp-6-5067-2006, URL <http://www.atmos-chem-phys.net/6/5067/2006/>, 2006.
- Jöckel, P., Kerkweg, A., Buchholz-Dietsch, J., Tost, H., Sander, R., and Pozzer, A.: Technical Note: Coupling of chemical processes with the Modular Earth Submodel System (MESSy) submodel TRACER, *Atmos. Chem. Phys.*, 8, 1677–1687, doi:10.5194/acp-8-1677-2008, URL <http://www.atmos-chem-phys.net/8/1677/2008/>, 2008.
- Jöckel, P., Kerkweg, A., Pozzer, A., Sander, R., Tost, H., Riede, H., Baumgaertner, A., Gromov, S., and Kern, B.: Development cycle 2 of the Modular Earth Submodel System (MESSy2), *Geosci. Model Dev.*, 3, 717–752, doi:10.5194/gmd-3-717-2010, URL <http://www.geosci-model-dev.net/3/717/2010/>, 2010.
- Jöckel, P., Tost, H., Pozzer, A., Kunze, M., Kirner, O., Brenninkmeijer, C. A. M., Brinkop, S., Cai, D. S., Dyroff, C., Eckstein, J., Frank, F., Garny, H., Gottschaldt, K.-D., Graf, P., Grewe, V., Kerkweg, A., Kern, B., Matthes, S., Mertens, M., Meul, S., Neumaier, M., Nützel, M., Oberländer-Hayn, S., Ruhnke, R., Runde, T., Sander, R., Scharffe, D., and Zahn, A.: Earth System Chemistry integrated Modelling (ESCiMo) with the Modular Earth Submodel System (MESSy) version 2.51, *Geosci. Model Dev.*, 9, 1153–1200, doi:10.5194/gmd-9-1153-2016, URL <http://www.geosci-model-dev.net/9/1153/2016/>, 2016.
- Kerkweg, A. and Jöckel, P.: The 1-way on-line coupled atmospheric chemistry model system MECO(n) - Part 2: On-line coupling with the Multi-Model-Driver (MMD), *Geosci. Model Dev.*, 5, 111–128, doi:10.5194/gmd-5-111-2012, URL <http://www.geosci-model-dev.net/5/111/2012/>, 2012.
- Kerkweg, A., Buchholz, J., Ganzeveld, L., Pozzer, A., Tost, H., and Jöckel, P.: Technical Note: An implementation of the dry removal processes DRY DEPosition and SEDimentation in the Modular Earth Submodel System (MESSy), *Atmos. Chem. Phys.*, 6, 4617–4632, doi:10.5194/acp-6-4617-2006, URL <http://www.atmos-chem-phys.net/6/4617/2006/>, 2006a.
- Kerkweg, A., Sander, R., Tost, H., and Jöckel, P.: Technical note: Implementation of prescribed (OFFLEM), calculated (ONLEM), and pseudo-emissions (TNUDGE) of chemical species in the Modular Earth Submodel System (MESSy), *Atmos. Chem. Phys.*, 6, 3603–3609, doi:10.5194/acp-6-3603-2006, URL <http://www.atmos-chem-phys.net/6/3603/2006/>, 2006b.
- Kotlarski, S., Keuler, K., Christensen, O. B., Colette, A., Déqué, M., Gobiet, A., Goergen, K., Jacob, D., Lüthi, D., van Meijgaard, E., Nikulin, G., Schär, C., Teichmann, C., Vautard, R., Warrach-Sagi, K., and Wulfmeyer, V.: Regional climate modeling on European scales: a joint standard evaluation of the EURO-CORDEX RCM ensemble, *Geosci. Model Dev.*, 7, 1297–1333, doi:10.5194/gmd-7-1297-2014, URL <http://www.geosci-model-dev.net/7/1297/2014/>, 2014.

- Landgraf, J. and Crutzen, P. J.: An efficient method for online calculations of photolysis and heating rates., *J. Atmos. Sci.*, 55, 863–878, doi:<http://dx.doi.org/10.1175/1520-0469>, 1998.
- Pozzer, A., Jöckel, P., Sander, R., Williams, J., Ganzeveld, L., and Lelieveld, J.: Technical Note: The MESSy-submodel AIRSEA calculating the air-sea exchange of chemical species, *Atmos. Chem. Phys.*, 6, 5435–5444, doi:10.5194/acp-6-5435-2006, URL <http://www.atmos-chem-phys.net/6/5435/2006/>, 2006.
- Roeckner, E., Bäuml, G., Bonaventura, L., Brokopf, R., Esch, M., Giorgetta, M., Hagemann, S., Kirchner, I., Kornbluh, L., Manzini, E., Rhodin, A., Schlese, U., Schulzweida, U., and Tompkins, A.: The atmospheric general circulation model ECHAM5. PART I: Model description, MPI-Report 349, Max Planck Institut für Meteorologie in Hamburg, Deutschland, available at: https://www.mpimet.mpg.de/fileadmin/publikationen/Reports/max_scirep_349.pdf (last access: 18 October 2015), 2003.
- Roeckner, E., Brokopf, R., Esch, M., Giorgetta, M., Hagemann, S., Kornbluh, L., Manzini, E., Schlese, U., and Schulzweida, U.: Sensitivity of Simulated Climate to Horizontal and Vertical Resolution in the ECHAM5 Atmosphere Model, *J. Climate*, 19, 3771–3791, doi:10.1175/jcli3824.1, URL <http://dx.doi.org/10.1175/jcli3824.1>, 2006.
- Sander, R., Baumgaertner, A., Gromov, S., Harder, H., Jöckel, P., Kerkweg, A., Kubistin, D., Regelin, E., Riede, H., Sandu, A., Taraborrelli, D., Tost, H., and Xie, Z.-Q.: The atmospheric chemistry box model CAABA/MECCA-3.0, *Geosci. Model Dev.*, 4, 373–380, doi:10.5194/gmd-4-373-2011, URL <http://www.geosci-model-dev.net/4/373/2011/>, 2011.
- Tost, H., Jöckel, P., Kerkweg, A., Sander, R., and Lelieveld, J.: Technical note: A new comprehensive SCAVenging submodel for global atmospheric chemistry modelling, *Atmos. Chem. Phys.*, 6, 565–574, doi:10.5194/acp-6-565-2006, URL <http://www.atmos-chem-phys.net/6/565/2006/>, 2006a.
- Tost, H., Jöckel, P., and Lelieveld, J.: Influence of different convection parameterisations in a GCM, *Atmos. Chem. Phys.*, 6, 5475–5493, doi:10.5194/acp-6-5475-2006, URL <http://www.atmos-chem-phys.net/6/5475/2006/>, 2006b.
- Tost, H., Jöckel, P., and Lelieveld, J.: Lightning and convection parameterisations – uncertainties in global modelling, *Atmos. Chem. Phys.*, 7, 4553–4568, doi:10.5194/acp-7-4553-2007, URL <http://www.atmos-chem-phys.net/7/4553/2007/>, 2007.
- Tost, H., Lawrence, M. G., Brühl, C., Jöckel, P., Team, T. G., and Team, T. S.-O.-D.: Uncertainties in atmospheric chemistry modelling due to convection parameterisations and subsequent scavenging, *Atmos. Chem. Phys.*, 10, 1931–1951, doi:10.5194/acp-10-1931-2010, URL <http://www.atmos-chem-phys.net/10/1931/2010/>, 2010.